



Synthesis of a poly(*p*-aminophenol)/starch/graphene oxide ternary nanocomposite for removal of methylene blue dye from aqueous solution

Hani K. Ismail¹ · Layth I. Abd Ali¹ · Hasan F. Alesary² · Basim K. Nile³ · Stephen Barton⁴

Received: 10 October 2021 / Accepted: 3 April 2022 / Published online: 11 April 2022
© The Polymer Society, Taipei 2022

Abstract

In the current study, poly(*p*-aminophenol) (PpAP), with starch and graphene oxide (GO), was successfully synthesised by oxidative polymerisation from *p*-aminophenol monomer in an aqueous alkaline medium using ammonium persulfate (APS) as an oxidising agent. The synthesised polymers were characterised using UV–Vis spectroscopy, Fourier transform infrared spectroscopy, thermogravimetric analysis, X-ray diffraction (XRD), and Brunauer–Emmett–Teller and zeta potential techniques. These techniques confirmed the presence of site-selective interaction between the conjugated PpAP chain and π -bonded surface, and thus the H-bonding of starch and GO. Further, the enhanced dye removal efficiency was ascribed to the improved morphology and the pore volume created by the entangled PpAP/Starch/GO. The influences of experimental conditions, such as the polymer composite content, dye concentration, time, pH of the bath solution, and temperature on cationic dye adsorption, were investigated. The adsorption data were fitted to the Langmuir isotherm (R^2 in the range between 0.997 and 0.9995) and showed a pseudo-second order (R^2 = in the range of 0.996 to 0.9996) kinetic model. Moreover, the polymer ternary composite was able to remove a large proportion (96.7%) of the cationic dye from water at pH 7. The thermodynamic investigation found that the adsorption process was spontaneous and endothermic. In addition, the synthesised adsorbent showed good reusability at six cycles. The data acquired suggest that the PpAP/Starch/GO composite can be effectively applied and reused as an inexpensive adsorbent material for removal of MB dye from water.

Keywords Adsorption · Colour removal · Methylene blue · Polymer nanocomposite

Introduction

Water is the basis for the survival of all living species on earth. Generally, the presence of dyes in water reduces the amount of dissolved oxygen and increases the demand for biochemical oxygen; thus, this affects the sustainability of aquatic life [1, 2]. Wastewater contaminated with dyes is

considered one of the most significant pollutants from the various industrial sources that cause severe environmental pollution. Many manufacturers of plastics, rubber, textiles, leather, paper, cosmetics, and food use dyes in their products, and the disposal of even small amounts of such can affect the ecosystem and result in serious environmental problems [3, 4]. Therefore, removing dyes from wastewater is an important route to significantly reducing water and soil pollution. In this regard, investigators have used a range of traditional methods, such as coagulation, mass reduction, biodegradation, adsorption, ion exchange, and advanced oxidation, to remove dyes and pigments from wastewater [5–7]. However, adsorption typically represents a much more economic approach due to the fact that this technique is characterised by its ease of use, the simplicity of the method, and its high efficiency [8, 9].

A variety of adsorbents to remove dyes from wastewater have been suggested in the literature, such as carbon-based substances, metal oxide nanocomposites [10, 11],

✉ Hani K. Ismail
hani.khalil@koyauniversity.org

¹ Department of Chemistry, Faculty of Science and Health, Koya University, Koya KOY45, Kurdistan Region - F.R., Iraq

² Department of Chemistry, College of Science, University of Kerbala, Karbala, Iraq

³ Engineering College, University of Kerbala, Karbala 56100, Iraq

⁴ School of Life Sciences, Pharmacy and Chemistry, Kingston University London, Kingston-Upon-Thames, Surrey, UK

clay materials [12], zeolites [13], and chitosan [14]. In the past few years, graphene-based carbon substances such as graphene oxide (GO is a derivative of graphite) have been widely investigated for dye adsorption due to the fact that they have large surface areas and numerous functional groups of potential utility, for instance hydroxyl (- OH), epoxy (- C—O—C), carboxyl (- COOH), and hydrophilic groups. The existence of these functional groups allows GO to easily interact with inorganic and organic substances via non-covalent interactions or covalent bonding, resulting in good adsorptivity of heavy metal ions and cationic dyes. Moreover, the unique 2-D structure of GO has high dispersion ability in aqueous solutions due to increased interplanar distance or weakened interplanar π - π interactions [15]. However, their adsorption effectiveness may decrease due to the reassembly of graphene nanosheets as a result of strong π - π stacking reactions, resulting in a difficult separation from water after pollutant adsorption [16, 17]. Recently, some new polymer materials, typically involving polypyrrole (PPy) and polyaniline (PANI) and their derivatives, have attracted considerable attention with regard to the removal of dyestuffs, pigments, and various forms of pollutant from water. These polymers have low fabrication costs and are important electrical conductors with various potential applications, as reported in the literature [18–20]. They can be effectively used to adsorb dyes, heavy metal ions, and various pollutants from wastewater/aqueous solutions. This is due to the fact that they are low cost, semi-flexible, and have unique electrical and optical properties. Nevertheless, these polymers suffer from certain disadvantages such as poor mechanical strength, low surface area, low porosities, and low cycle life stabilities. As a result, they swell and shrink during ion exchange processes, restricting their range of practical applications [6, 7].

In addition, carbohydrate polymers (starch, cellulose, chitosan, alginate, dextran, etc.) are extensively employed as adsorbents for the removal of dyestuffs from wastewater due to their low-cost, non-toxicity, biodegradability, and their physical and chemical properties resulting from the presence of hydroxyl, carboxyl, amine, and amide functional groups, which facilitate the adsorption of dyes through hydrogen bonding and electrostatic interactions [21]. Therefore starch is an appropriate organic agent for surface modification to improve the morphology of the polymer matrix [22]. Adsorbent nanocomposites based on polymeric materials have excellent characteristics due to their environmental stability, high surface areas, large pore volumes, and effective binding sites [23]. As a result, polymeric adsorbents based on organic composites/nanocomposites have been used for the adsorption of dyestuffs from aqueous solution. Many reports have been published on the synthesis of polymers modified with starch and/or carbonaceous materials for dye removal; for example, Janaki et al. [24] prepared starch/

polyaniline nanomaterials via in situ polymerisation for removal of different dyes compounds from aqueous solution, while Gomes et al. [25] synthesised starch/cellulose nanowhisker hydrogel composites to eliminate methylene blue (MB) from wastewater. Cheng et al. synthesised [26] a dithiocarbamate-modified starch adsorbent to adsorb anionic dyes from aqueous solutions. Furthermore, Starch/Multi-Walled Carbon Nanotube (MWCNT)-Valine (SMV) nanocomposites [22] and Fe₃O₄-based starch-poly(acrylic acid) [27], starch-g-polymethyl methacrylate [28], were used as adsorbents for environmental treatment. Thus, polymers have been used with graphene oxide, for example, polyaniline/graphene oxide [29], graphene oxide/silver phosphate, polyurethane nanocomposite [30], polyacrylic acid functionalized magnetic iron oxide nanoparticle-graphene oxide nanocomposites [31], and polypyrrole-cellulose-graphene oxide nanocomposites [32]. In our previous work, we prepared a new nanocomposite adsorbent based on a polyaniline/manganese oxide/nickel oxide composite which showed good adsorption capacity for removal of methyl orange dye from water (248.4 mg/g) [33].

In this study, poly(*p*-aminophenol), and starch were successfully fabricated with graphene oxide sheets via an in situ chemical oxidation polymerisation process to produce PpAP/starch/GO ternary nanocomposites for the removal of cationic methylene blue (MB) from aqueous solution. The *p*-aminophenol monomer was chosen due to its two functional groups (NH₂ and OH) supplying a greater number of reactive groups than other monomers such as pyrrole and aniline, which have amine groups only. Starch is a biocompatible polysaccharide and is employed for the construction of nanocomposites due to its advantageous biological and molecular properties. The functionalization of PpAP and starch can be achieved via cross-linking their amino and hydroxyl groups to the epoxy groups present in GO, with the resulting composite offering tremendous potential in terms of its numerous potential applications. Accordingly, the PpAP/starch/GO ternary nanocomposite is relatively rich in surface functional groups including amino, carboxyl, and hydroxyl groups, and hence it can more effectively adsorb dyes from aqueous solution. To the best of our knowledge, this new modification of the PpAP/starch/GO ternary nanocomposite has never been utilised for the adsorption of dyes. The binding of PpAP/starch/GO ternary nanocomposites was examined via different techniques such as X-ray diffraction (XRD), scanning electron microscopy (SEM), transmission electron microscopy (TEM), thermo-gravimetric analysis (TGA), Fourier transform infrared (FTIR) spectroscopy, Brunauer–Emmett–Teller (BET), and zeta potential. The influence of various factors such as initial concentration of dye, adsorbent dosage, contact time, pH, and temperature on adsorption efficiency were also determined in this work. In addition, the adsorption data were fitted with kinetic and

thermodynamic models as well as isotherm mechanisms. The data show that the PpAP/Starch/GO ternary can act as an effective adsorbent for the purposes of water purification.

Experimental

Materials and reagents

The materials used in this study were as follows: *p*-aminophenol (99%), starch (98%), ammonium persulfate (APS, 98%), and sulfuric acid (95%) were used as received from Aldrich; graphite powder (99%) from Alfa Aesar; methylene blue (MB, C₁₆H₁₈ClN₃S·xH₂O, molecular weight: 319.85 g/mol), sodium hydroxide (NaOH, 97%), sodium nitrate (NaNO₃, 99.5%), hydrogen peroxide (H₂O₂, 30%), hydrochloric acid (HCl, 37%), and dimethyl sulfoxide (DMSO, 99.9%) were used from Merck without further purification. Double distilled water was used for washing and preparation purposes.

Sample preparation

Synthesis of graphene oxide (GO)

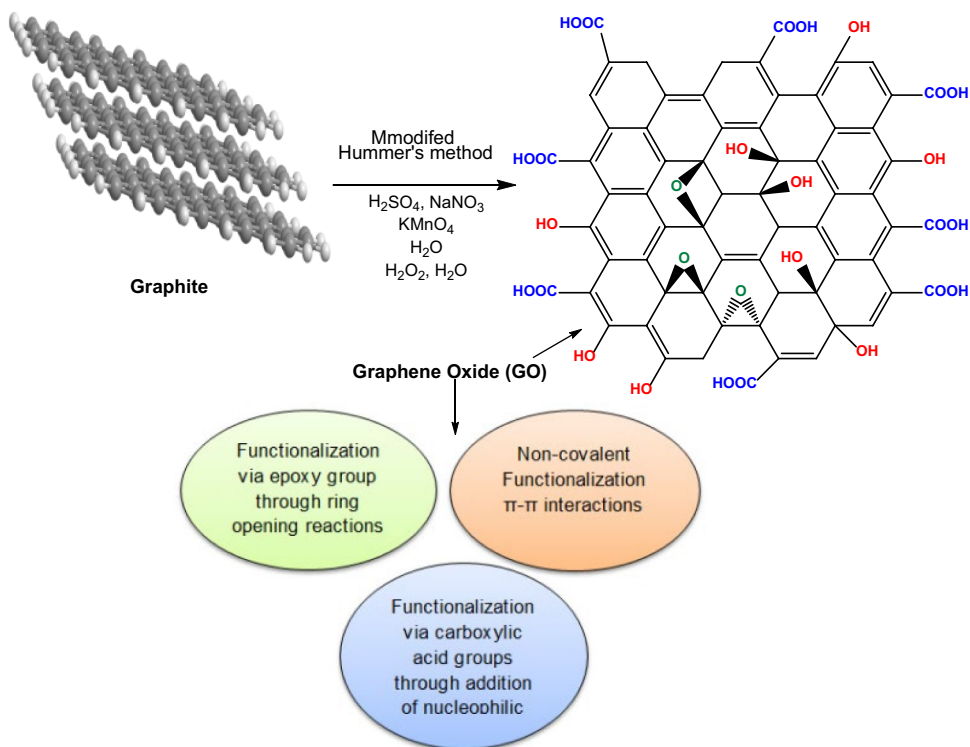
Graphene oxide was prepared from graphite powder following a modified Hummer's procedure [34], and the proposed structure is shown in Fig. 1. In a typical method, 4.0 g of graphite powder was added into a 500 mL flask followed by

adding 92 mL of concentrated H₂SO₄ and, thereafter, 2.0 g of NaNO₃. Then, the mixture was placed in an ice bath and stirred by a magnetic stirrer for 30 min. Subsequently, 12 g of KMnO₄ as an oxidising agent was added slowly to the mixture, keeping the reaction temperature to less than 20 °C. The mixture was then removed from the ice bath and left overnight at 25 ± 2 °C with continuous stirring. A brownish paste product was formed; next, 150 mL of distilled water was slowly added to the product under strong stirring. The temperature of the mixture increased to 98 °C (exotherm produced), after which it was allowed to cool to room temperature. Then, the mixture was treated with 10 mL of H₂O₂ and the colour of the mixture changed from dark brown to yellow, resulting in an oxidation product of GO produced from the graphite. The GO product was washed with 2 M HCl aqueous solution followed by distilled water until the pH of the washing solution was nearly neutral. Finally, the GO product was acquired as a solid powder after filtration and drying under vacuum and used to prepare the polymer composite, as illustrated in Fig. 3.

Synthesis of PpAP/Starch/GO adsorbent

PpAP/Starch/GO adsorbent was synthesised by oxidative polymerisation of *p*-aminophenol (*p*AP) monomer in an aqueous alkaline (NaOH) medium using ammonium persulfate (APS) as an oxidising agent, as shown in Fig. 2, according to the procedure described in the literature [35, 36] with some modification. In a typical procedure, 6.9 g of

Fig. 1 Proposed graphene oxide structure as prepared from graphite



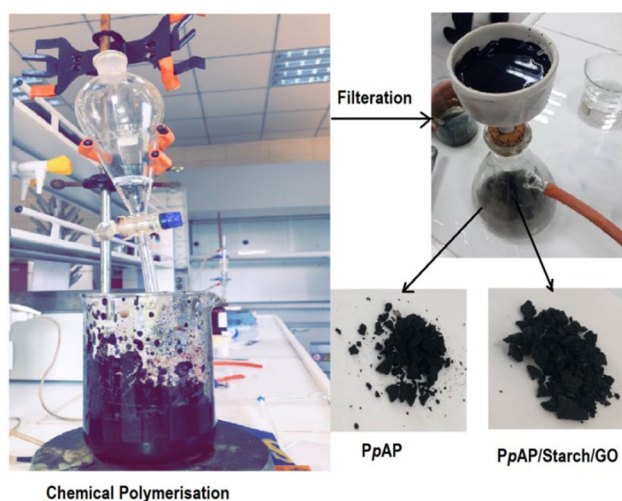


Fig. 2 Photographic image of the polymerisation process in the lab

*p*AP was dissolved in 100 mL aqueous 0.6 M NaOH medium by continuous magnetic stirring for 30 min. Thereafter, 2.3 g of starch powder was added to the monomer solution synthesised in advance (6.9 g of *p*AP was dissolved in 100 ml aqueous 0.6 M NaOH medium) containing different percentage weights of graphene oxide (GO). These solutions were stirred for 30 min and then sonicated via a probe ultrasonicator for 1 h to form a homogenous solution. The mass ratio of *p*AP monomer to starch powder was 75:25, respectively, containing different percentage weights of GO (viz. 2, 4, 6, 8 and 10 wt%) with respect to the *p*AP monomer and starch (3:1). After that, fresh APS solution was prepared by dissolving 20.54 g APS in 50 ml distilled water. The polymerisation was performed in the conventional method via dropwise addition of the oxidant (APS solution) into the mixture (i.e., monomer + starch + GO) over 4 h, with the mixture continuously reacting at room temperature (25 ± 2 °C) with constant stirring for 24 h. At the end of this process, the resultant black precipitate was separated by filtration and washed with 250 mL HCl (1 M) to remove by-products, soluble oligomers, unreacted monomer and other materials, followed by further washes with a considerable quantity of distilled water until a clear washing solution was obtained. The product was subsequently dried in a vacuum oven at 60 °C for 24 h. The yield of the dried polymer composite was 92.1%.

The chemical polymerisations for pure *p*AP monomer and *p*AP mixed with various mass ratios of starch (see Table 1) were carried out as per the strategy used for PpAP/Starch/GO illustrated above but without adding GO. The product was subsequently dried at 60 °C for 24 h. The yield of the dried pure PpAP polymer was 65.7% while those for PpAP mixed with starch samples were between 71 and 84%. The mechanism of formation of poly(*p*-aminophenol), starch,

Table 1 Optimisation of PpAP nanocomposite for methylene blue dye removal ($C_i = 100$ mg/L), time = 60 min, $V = 100$ mL, dose = 50 mg) from aqueous solution

Samples	Composite			Dye removal %
	PpAP (g)	Starch (g)	GO (g)	
1	10	0	0	33
2	8.57	1.43	0	38
3	7.5	2.5	0	55
4	6.0	4.0	0	53
5	5.0	5.0	0	50
6	(PpAp@Starch 3:1) 9.8	0.2	0	65
7	(PpAp@Starch 3:1) 9.6	0.4	0	74
8	(PpAp@Starch 3:1) 9.4	0.6	0	85
9	(PpAp@Starch 3:1) 9.2	0.8	0	91
10	(PpAp@Starch 3:1) 9.0	1.0	0	89

and graphene oxide via the chemical polymerisation process is illustrated in Fig. 3.

Determination of the amount of water absorbed

The amount of water absorbed by the polymer composite was determined simply by weighing the polymer before and after absorbing water. Certain amounts of the polymers (samples 1 and 9, see Table 1) were each placed in 25 mL distilled water; the samples were then left for 24 h in continuously stirred water. Then, the remaining water was removed by centrifugation and the wet samples were weighed. The percentage of water ($W\%$) absorbed by the polymers was calculated from Eq. 1 [14]:

$$W\% = \frac{W_w - W_d}{W_w} 100 \quad (1)$$

where W_d and W_w are weights (g) of the dried and wet yields, respectively. The amounts of water absorbed by pure PpAP and PpAP/Starch/GO were $44 \pm 2\%$ and $34 \pm 2\%$, respectively, which indicate that the adsorbents have hydrophilic features based on the experimental conditions.

Batch adsorption experiments

Adsorption tests were achieved with batch mode to compute the adsorption efficiency of ternary PpAP/starch/GO nanocomposites. Adsorption kinetics assays were performed in the presence of a known quantity of ternary nanocomposite sample at pH 7 and at 298 K. In the kinetic assays, different initial concentrations of MB dye of 10, 75 and 150 mg/L were employed. Standard conical flasks containing a specified dose of ternary nanocomposites (50 mg) and 100 mL of MB dye samples were shaken in an orbital shaker (G

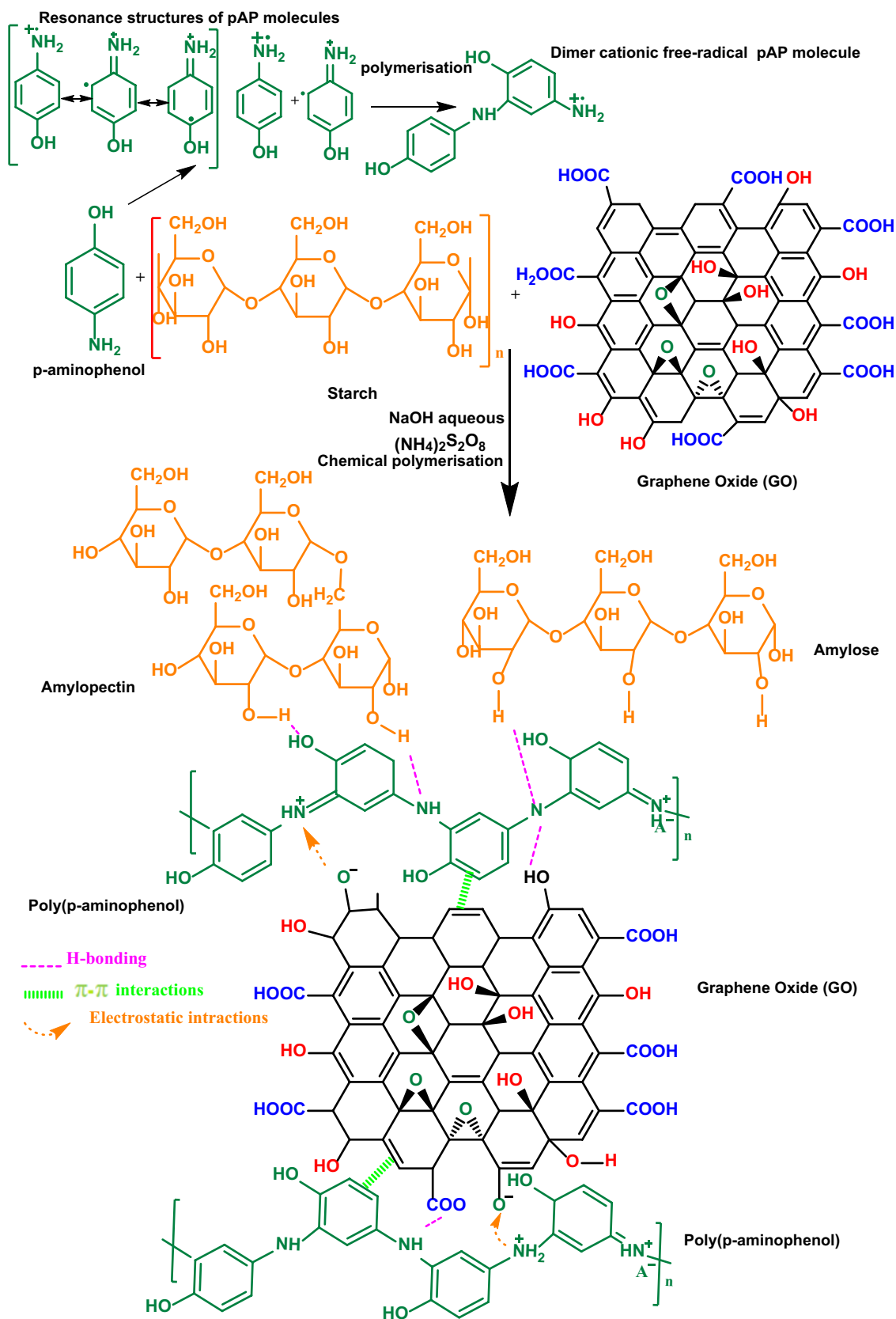


Fig. 3 Schematic of the proposed mechanism of synthesis of the PpAP/starch/GO ternary nanocomposites

BIOSCIENCES) at a fixed shaking rate of 200 rpm. Ternary nanocomposite aliquots were removed from the 250 mL standard conical flasks at indicated sorption times, and the remaining MB dye concentrations were detected at 664 nm using a high-performance UV–vis (Agilent Cary 5000) spectrophotometer. While adsorption isotherm assays were performed at pH 7, the optimum weight of the ternary nanocomposites (50 mg) was mixed with 100 mL MB dye solution with different initial concentrations in the range 10–200 mg/L for 60 min at 298, 310, and 320 K.

The quantities of adsorbed MB dye per gram of ternary nanocomposites at time t , q_t (mg/g) and at equilibrium, q_e (mg/g) were computed using Eqs. (2) and (3), respectively:

$$q_t = \frac{(C_i - C_t)V}{M} \quad (2)$$

$$q_e = \frac{(C_i - C_e)V}{M} \quad (3)$$

where C_i (mg/L) and C_t (mg/L) are the MB dye concentrations at time 0 and at time t , respectively, V (L) refers to the volume of MB dye solution, M (g) refers to the mass of the ternary nanocomposites, and C_e (mg/L) is related to the dye concentration at equilibrium. Moreover, the average adsorption of three determinations as well as the relative errors of the experimental results were less than 5%.

The percentage of MB removed (*MB Removal %*) was determined using Eq. (4), as follows:

$$MB \text{ Removal } \% = \frac{(C_i - C_e)}{C_i} \times 100 \quad (4)$$

Influences of experimental factors on the adsorption in the MB process

In this investigation, the influences of initial solution pH (in the range 2–10), adsorbent dose (in the range 10–80 mg), initial MB dye concentration (in the range 10–200 mg/L), and sorption time were examined.

Instrumentations and characterisations

The polymers synthesised in this study were characterised via the UV–Vis, FTIR, TGA, XRD, SEM, TEM, and BET techniques. Typically, Fourier transform infrared (FTIR) spectra were used to elucidate the functional groups present in the samples (*PpAP* and *PpAP* composite). The sample powders were dispersed in KBr pellets and FTIR spectra recorded in the range 500 to 4000 cm^{-1} using a Perkin Elmer Spectrum One Fourier Transform Infrared spectrophotometer. The UV–Vis spectra of the polymer composites were measured using a Cary Series UV–Vis spectrophotometer

(Agilent Technologies) after dissolving the polymers in dimethyl sulfoxide (DMSO) in quartz cuvettes, with spectra measured in the wavelength range 200–800 nm. The thermal stability was characterised as a function of the temperature for the polymer powders via Thermo-Gravimetric Analysis (TGA) using a Mettler Toledo 44 TGA/DSC 1 STARE machine. The weight of each sample used was between 15–20 mg in open aluminium pans. The STARE system software was utilised to obtain the percentage mass loss from the raw data analysis, which was then replotted. The crystal structures of the polymer composites were examined using an X-ray spectrometer, model: Panalytical Empyrean with 30 mA, 45 kV, and scanned between 5° and 80° 2 θ . A Phillips XL30 ESEM instrument with an accelerator voltage of 15 keV and transmission electron microscope (TEM) PHILIPS CM120 were used to characterise the surface morphology of the pure *PpAP* and *PpAP*/starch/GO ternary composites. The pore size and the pore diameter distributions for the polymer composite were determined by Barret–Joyner–Halenda (BJH), whereas the specific pore volume and the specific surface area for polymer composite were measured via the Brunauer–Emmett–Teller (BET) method. For the determination of the zero-point charges (pH_{ZPC}) of the ternary nanocomposites, the pH for the zero-point charges (pH_{zpc}) can be measured by performing a pH drift procedure. In a series of 250 mL volumetric flasks, each containing 50 mL NaNO_3 (0.1 mol/L), 50 mg *PpAP*/starch/GO ternary nanocomposite was added. The different initial pH (pH_i) between 2 to 11 was adjusted with a solution of HCl (0.1 mol/L) or NaOH (0.1 mol/L). The final solution pHs (pH_f) were determined after 48 h equilibration. The pH_{PZC} value was verified from a plot of ΔpH ($\Delta\text{pH} = \text{pH}_f - \text{pH}_i$) against pH_i at $\Delta\text{pH} = 0$.

Results and discussion

Optimisation of polymer composite as an adsorbent

In this study, several samples of *PpAP* composite were prepared according to the procedure described in the experimental section in order to obtain the best integrated polymer composite for the adsorption of MB dye from aqueous solution. Table 1 shows the optimised weight ratio of starch and GO in the *PpAP* composites. From this table, the lowest value for removal of MB was pure *PpAP* (33% sample 1), while increasing the amount of starch in the polymer composite increased the percentage removal of MB dye as a result of the increase in the number of active sites in the polymer composite, recording a higher removal of MB dye of 55% for sample 3 (*PpAP*@Starch at a ratio of 3:1). Further, it was found that there was a small decline in the adsorption effectiveness of MB when the amount of starch was greater

than 25 wt% in the PpAP composite used (samples 4 and 5). This might suggest that starch molecules agglomerated with the polymer, reducing the ability of the adsorbent to remove MB from aqueous solution.

After this step, samples 6–10 performed by addition various percentage weights of GO sheets (viz. 2, 4, 6, 8 and 10 wt%) to the pAP monomer and starch powder (the mass ratio of pAP monomer to starch powder was 3:1, which was selected from sample 3). It is clear that there is an increase in the adsorption of MB dye with increasing GO content in the polymer composite, showing the highest removal of dye was 91% for sample 9 (the mass ratio between PpAp@Starch (3:1) and GO was 92:8%, respectively). This is because of the synergistic effects between PpAP, starch molecules, and graphene oxide sheets, which led to an enhancement of the porous nature of the structure of the ternary composite (as indicated in the BET results) during this optimisation process, and which allowed the surface of PpAP/Starch/GO ternary composite to adsorb MB dye highly effectively via its pores. The high dye-removing performance is also related to the large number of functional groups present in the ternary composite which enhance electrostatic reactions, hydrogen bonding, and π - π interactions between the MB dye and the ternary composite, as shown in the schematic (Fig. 4b). Figure 4a (right) displays a photo of a deep blue colour in the MB solution ($C_i = 100$ mg/L) prior to the addition of the adsorbent (sample 9). After the adsorbent has been allowed to act for 60 min, the colour of the MB solution had changed to a transparent light blue (nearly colourless, Fig. 4a (left)) due to the adsorption process, implying the majority of MB solution had been removed by the adsorbent (sample 9). Depending on these results, sample 9 was selected as the best adsorbent to study the mechanism of the removal of MB from aqueous solution.

Characterisation of the adsorbents

Based on the optimisation results, as presented in Table 1, the pure PpAP (sample 1) and PpAP/Starch/G (sample 9) samples were selected for the characterisation of their respective structures, as follows:

X-ray diffraction (XRD) analysis

Figure 5 presents the X-ray diffraction patterns for PpAP and its nanocomposites (PpAP/Starch/GO), where X-ray diffraction can be used to determine the crystalline and amorphous regions in the polymers. Generally, an amorphous region in the matrix of a polymer is indicated by the presence of relatively broad low intensity peaks, whereas the crystalline region is characterised by peaks with sharp intensities. Herein, the PpAP shows broad scattering at 2θ values between 15 and 30° (the broad maximum appears

at $2\theta = 23.66^\circ$), which is attributed to the periodicity parallel and perpendicular to the PpAP matrix, indicating its amorphous nature, as described for the PmAP doped with MWCNT [37]. In the instance of PpAP/Starch/GO nanocomposites (red line), the diffraction peaks observed and located at $2\theta = 15.42^\circ$, 17.17° , 22.53° , and 26.51° could be attributed to the (001), (011), (020), and (121) reflection planes, respectively, of PpAP nanocomposites, indicating that the PpAP/Starch/GO ternary composite was crystalline in nature. From these peaks, intensities were found to be increasing considerably with the addition of starch and GO to the polymer matrix. Accordingly, the two sharp diffraction peaks present at 22.53° and 26.51° in the sample (PpAP/Starch/GO) that were not observed in the pure PpAP sample correspond to the grafted crystalline structure of starch with PpAP due to increased intrachain hydrogen bonding or electrostatic interactions being present in the structures of the polymer with the starch (this includes amine, hydroxyl, and/or phenolic groups). Furthermore, the diffraction peaks for the GO layer (shown in the insert in Fig. 5) emerge at $2\theta = 15.79^\circ$ (001) relate to carboxyl, epoxy, and hydroxyl groups, and which is in agreement with previous reports in the literature [38]. The intensity of this peak decreased and shifted to lower degree in the polymer composite ($2\theta = 15.42^\circ$) due to the low GO content in polymer nanocomposites, suggesting GO layers combined with the PpAP matrix. This result showed that the crystallinity and orientation of the polymer ternary nanocomposites is of considerable interest, because more highly ordered systems can exhibit a polymeric conductive state and may have an impact on the removal of waste substances, as described in the following sections.

Fourier Transform Infrared Spectroscopy (FTIR) analysis

FTIR spectra of pure MB, pure PpAP, and the PpAP/Starch/GO ternary composite (before and after methylene blue adsorption) were recorded to study the functional groups present in the PpAP and the PpAP/Starch/GO composite, the results of which are presented in Fig. 6. For pure PpAP (black line), the broad peaks at 3160 and 2976 cm^{-1} can be attributed to the stretch vibrations of O–H and N–H. The bands at 1576 (weak) and 1488 cm^{-1} were assigned as characteristic stretching bands of the C=C bonds of quinoid and benzenoid structures in PpAP, respectively. Other peaks that could be attributed to PpAP were observed at 1360 , 1231 , 1057 , and 800 cm^{-1} due to C–N stretching vibrations (indicating the formation of a C–N–C structure in the polymers), C=C (in phenyl rings, which provided strong evidence for the presence of the *p*-aminophenol unit) and the C–H bending characteristic of aromatic ring substitution in the polymers, respectively [37, 39].

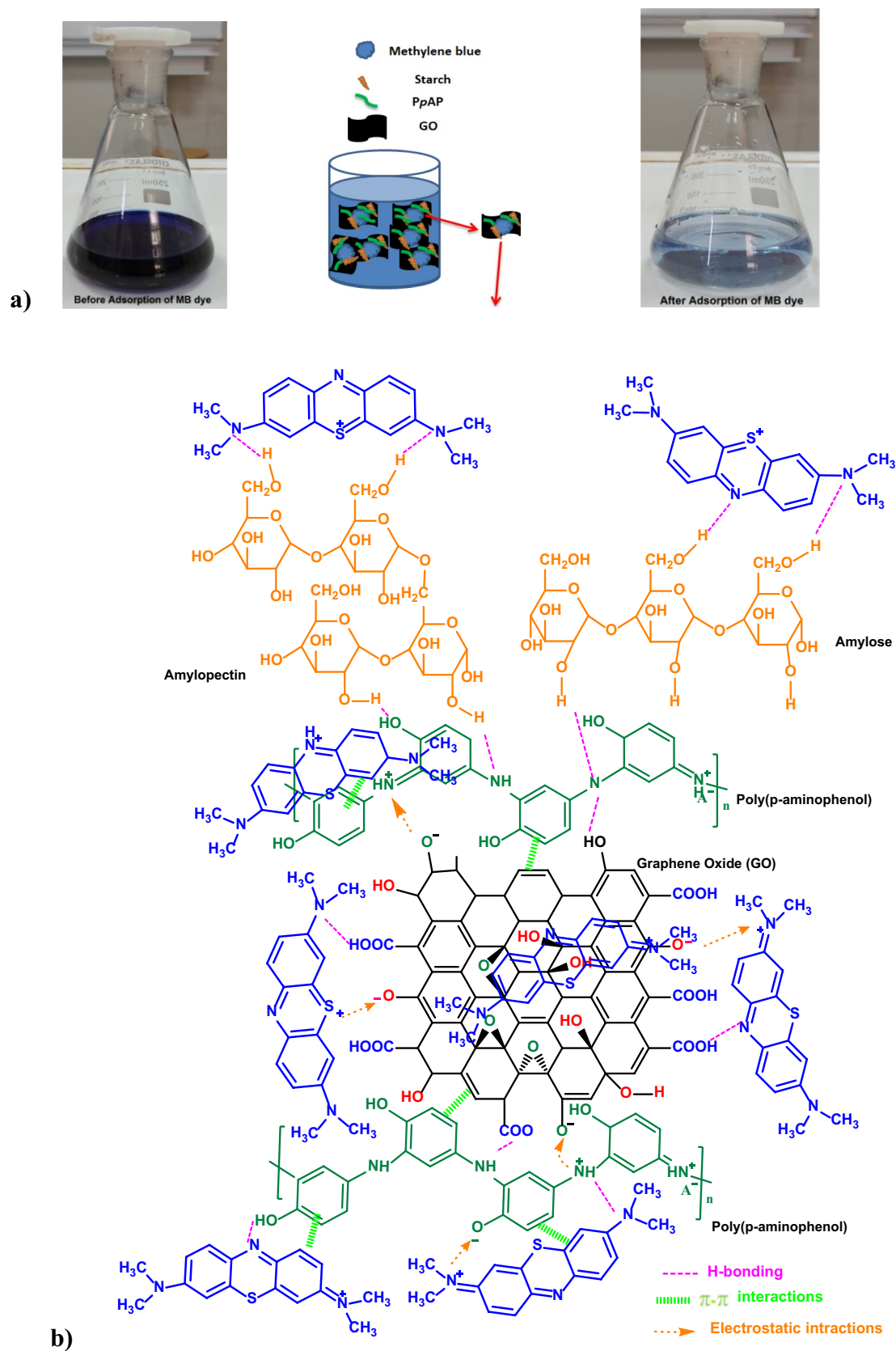


Fig. 4 a) images of methylene blue solution ($C_i=100$ mg/L) before and after MB removal, time=60 min, $V=100$ mL, dose=50 mg. b) Assumed schematic for removal MB cationic dye via the PpAP/Starch/GO ternary nanocomposite

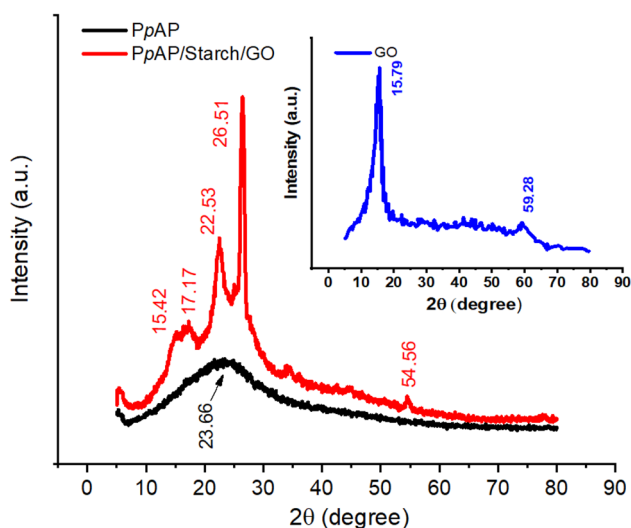


Fig. 5 XRD patterns of *PpAP* (black line), *PpAP/Starch/GO* (red line) and *GO* (inset, blue line)

The main evidence for formation of the complex comes from the differences between the FTIR spectra of the *PpAP/Starch/GO* composite (red line) and pure *PpAP* is the strong broad peak at 3421 (3664–3004) cm^{-1} , which is attributable to the O–H vibrations in starch and GO along with the N–H stretching vibration that generally appears in the IR spectrum of *PpAP* [35]. The C=C absorption bands for quinoid and benzenoid are shifted to 1552 and 1503 cm^{-1} , respectively, in the *PpAP/Starch/GO* structure. Thus, peaks of C–N–C, C=C and C–H in the polymer composite were shifted to 1369, 1254, and 1066 cm^{-1} , respectively, showing stronger and broader bands than those observed for the

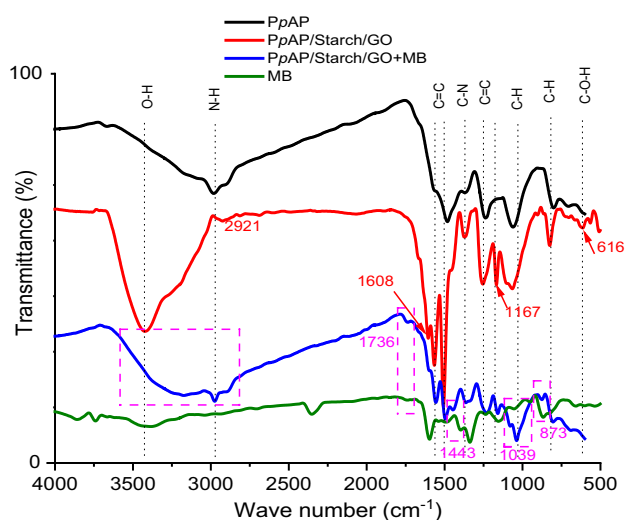


Fig. 6 FTIR spectra of *PpAP* and the *PpAP/Starch/GO* ternary nanocomposite powder

pure *PpAP* structure. In addition, there were new absorption bands observed in the *PpAP/Starch/GO* composite spectrum at 1608 cm^{-1} for the aromatic C=C vibrations of GO [40], while the bands at 1167 cm^{-1} and 616 cm^{-1} correspond to the C–O–H and C–O–C groups in starch [41], respectively. This indicated that *PpAP/Starch/GO* was successfully composited from *PpAP*, starch, and GO due to the presence of hydrophilic functional groups, for instance, carboxyl, epoxy, and hydroxyl groups, which suggests they provide good functional activity and are thus useful for the removal of cationic MB dyes. In conclusion, the interaction of starch and GO with the polymer was confirmed via FTIR, UV–Vis (see Fig. S1 in the supplementary material), and XRD characterisation.

After the *PpAP/Starch/GO* composite adsorbs the MB dye, it can be seen that the intensities of the adsorption bands for *PpAP/Starch/GO* (blue line) are weakened, which implies the suitable adsorption of MB by the polymer composite. Some additional peaks appeared in the FTIR at 1736 (indicative of the C=N⁺(CH₃)₂ stretching vibration), 1443 cm^{-1} (C=S⁺ bend), 1039 (C–NH–C bend), and 873 (C–S–C bend) cm^{-1} which are all related to functional groups found on MB [42, 43]. Moreover, there is a remarkable decrease in the intensity and shift in wavenumber of the broad peak at 3587–2838 cm^{-1} . The shift in the peaks and thus the alteration observed in the structure of *PpAP/Starch/GO* composite after adsorbing MB indicates that there was an interaction between the functional groups that exists in the *PpAP/Starch/GO* composite and the MB molecules.

Morphologic analysis

Transmission electron microscopy (TEM) and scanning electron microscopy (SEM) were performed to study the structures and surface morphologies of the *PpAP* and *PpAP/Starch/GO* nanocomposite (Fig. 7). Figure 7g depicts the SEM image of the GO structure before coating with the polymer and starch, as formed from graphite powder using the modified Hummers method. The GO sheets have the appearance of a somewhat thick, crumpled edge but after fabrication with *PpAP* and starch, its structure becomes more layered, presenting as very thin sheets, as shown in the TEM image (Fig. 7(h, i)). From the SEM images, it can be seen that the surface morphology of pure *PpAP* (Fig. 7b and c) is like lumped fibre particles with relatively low porosity (i.e., free volume) where the mean diameter of the *PpAP* fibres was about 58 nm, as shown in Fig. 7a (histogram plot).

The incorporation of starch and graphene oxide sheets into the *PpAP* matrix (Fig. 7e and its magnification (Fig. 7f)) produced a nanocomposite (*PpAP/Starch/GO*) with increased porosity, showing an uneven and lumpy surface associated with a number of cavities (increasing the cavities in the adsorbent facilitates the adsorption of dyes). The mean

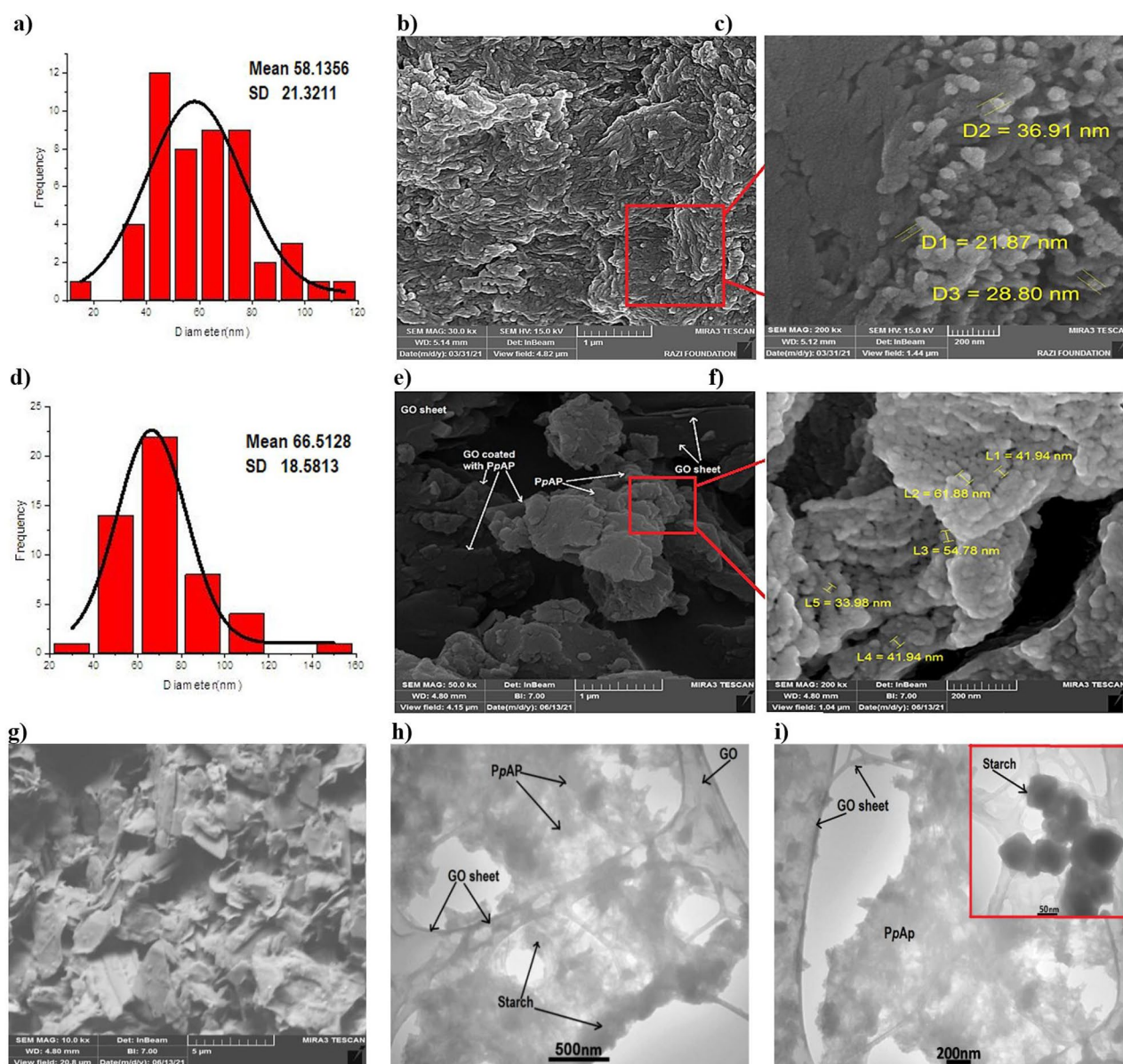


Fig. 7 Histogram plots of a pure PpAP **a)**, and PpAP/Starch/GO nanocomposite **d)**, with associated SEM images of a pure PpAP **b)**, **c)**, PpAP/Starch/GO nanocomposite **e)**, **f)** and GO **g)**. Images **h)** and **i)**

display TEM images of the PpAP/Starch/GO nanocomposite at different magnifications

diameter of the PpAP/Starch/GO nanostructure increased to about 66 nm after modification, as presented in Fig. 7d (histogram plot), confirming the nanocomposite structure of the prepared composite. SEM images of samples revealed that PpAP/Starch/GO nanostructure had more pores, which is consistent with its higher BET surface area (Supplementary material, Fig. S3). In addition, the SEM images of the nanocomposite sample clearly show the uniform coating of poly(*p*-aminophenol) and starch on the GO sheets. The variation in surface morphology of PpAP/Starch/GO occurs due to the grafting of GO sheets and starch molecules resulting in

aggregation and the formation of a network of PpAP chains via electrostatic and π - π interactions and hydrogen bonding as obtained between the starch, GO sheets, and PpAP due to the presence of large numbers of carboxyl, epoxy, and hydroxyl groups in their structures. This result was consistent with the XRD and FT-IR spectra of the PpAP/Starch/GO nanostructures. The TEM images (Fig. 7h) further confirm the nanocomposite structure of the as-synthesised nanoporous material. As shown in Fig. 7h, the typical TEM image clearly shows that the PpAP and starch nanocomposite are well anchored to the GO sheets in the nanostructure, which

is in accord with the SEM data. Thermogravimetric analysis showed that the thermal stability of the polymer composite was improved compared to that of PpAP, with associated data given in the supplementary material (Fig. S2).

Zero-point charge (pH_{zpc}) for ternary nanocomposites analysis

Zero-point charge is an important property in the prediction of the nature of the surface charge of adsorbent materials in solution in media at different pHs. Thus, according to the pH_{zpc} , one can potentially determine the pH that optimises MB dye adsorption. At a pH lower than pH_{zpc} , the adsorbed surface will be positively charged, and negatively charged when the pH of the aqueous samples is greater than pH_{zpc} . From the results presented in Fig. 8, the pH_{zpc} of the ternary PpAP/Starch/GO nanocomposites was determined to be 6. This means that the adsorbent PpAP/Starch/GO nanocomposites will show a positive charge surface in an aqueous sample when the pH is less than 6, which could be useful for the adsorption of anionic species, while a pH greater than 6 will result in a surface negative charge that is beneficial for the adsorption of cationic species. In addition, the pK_a of the MB dye is 3.8, so for aqueous samples at a pH greater than 3.8, the cationic MB species will be dominant [44]. Thus, the adsorption of MB dye molecules onto PpAP/Starch/GO nanocomposites would be most effective at a pH greater than 6.

Adsorption study of methylene blue dye

Influence of solution pH on MB dye adsorption

The influence of the pH of MB solution on the PpAP/Starch/GO ternary nanocomposite was observed by changing the reaction solution pH (in the range between 2 and 10). This demonstrated that the quantity of MB dye adsorbed by the PpAP/Starch/GO ternary nanocomposites (q_e (mg/g))

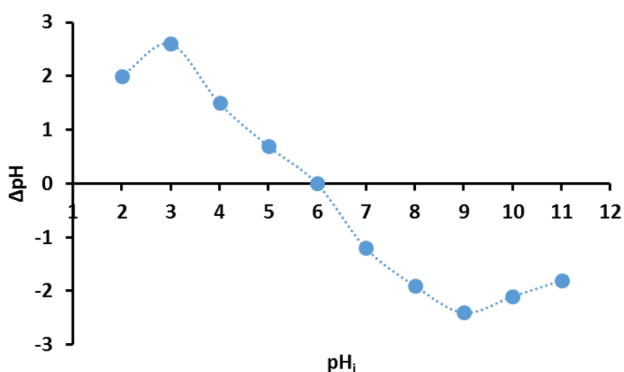


Fig. 8 Zero-point charge (pH_{zpc}) for ternary nanocomposites

increased with increasing solution pH (Fig. 9a). This trend was thought to be due to the participation of the electrostatic interactions between the cationic MB molecules adsorbate and the surface of the PpAP/Starch/GO ternary nanocomposite adsorbent. As specified above, the PpAP/Starch/GO ternary nanocomposites surface are positively charged at a pH below the pH_{zpc} of 6, and the adsorption of the positive MB dye molecules will thus be impeded by electrostatic repulsion. After the pH of the solution was increased to a neutral or alkaline pH, the electrostatic repulsion between the surface of the ternary PpAP/Starch/GO nanocomposites and the MB dye molecules accordingly decreased, resulting in more favourable conditions for adsorption [45, 46]. It was evident that the quantity of MD dye adsorbed by the PpAP/Starch/GO ternary nanocomposites (q_e (mg/g)) at pHs above the pH_{zpc} of 6 was significantly increased (reaching 194.2 mg/g at pH 7) due to increased electrostatic attraction, and then decreased slightly when further increasing the pH up to 10 (188.4 mg/g), perhaps because the rate of adsorption had reached saturation. A pH of 7 was accordingly selected for further sorption experiments.

Influence of adsorbent dose

The amount of adsorbent is one of the more significant factors in the economics of the batch adsorption process. The quantities of adsorbed MB dye (q_e (mg/g)) with different doses of adsorbent are shown in Fig. 9b. The quantities of MB dye adsorbed by the PpAP/Starch/GO ternary nanocomposites (q_e (mg/g)) increased from 44.6 with 10 mg adsorbent to a maximum of 193.2 with 50 mg adsorbent. A higher mass of 50 mg increases the total number of adsorbent species with increasing dose of nano-sorbents, leading to an increase in the associated number of active sites and surface area [47]. However, further increasing the mass of nanocomposites to 80 mg resulted in a slight decrease in sorption capacity (192.2 mg/g). This finding suggests that aggregation of the PpAP/Starch/GO ternary nanocomposites may have occurred at higher doses, leading to a lower surface area being available for sorption and for a longer diffusional path of MB molecules.

Influence of initial MB dye concentration

The quantities of MB dye adsorbed by the PpAP/Starch/GO ternary nanocomposites (q_e (mg/g)) was evaluated using several initial concentrations of MB dye in the range of 10 to 200 mg/L under optimal experimental conditions (initial pH 7, adsorbent dose 50 mg, sorption time 60 min, and temperature 298 K). Figure 9c shows that an increase in the initial MB dye concentration led to an increase in the quantity of MB dye adsorbed (q_e (mg/g)), indicating that the adsorption capacity increases at high MB dye concentrations. Previous

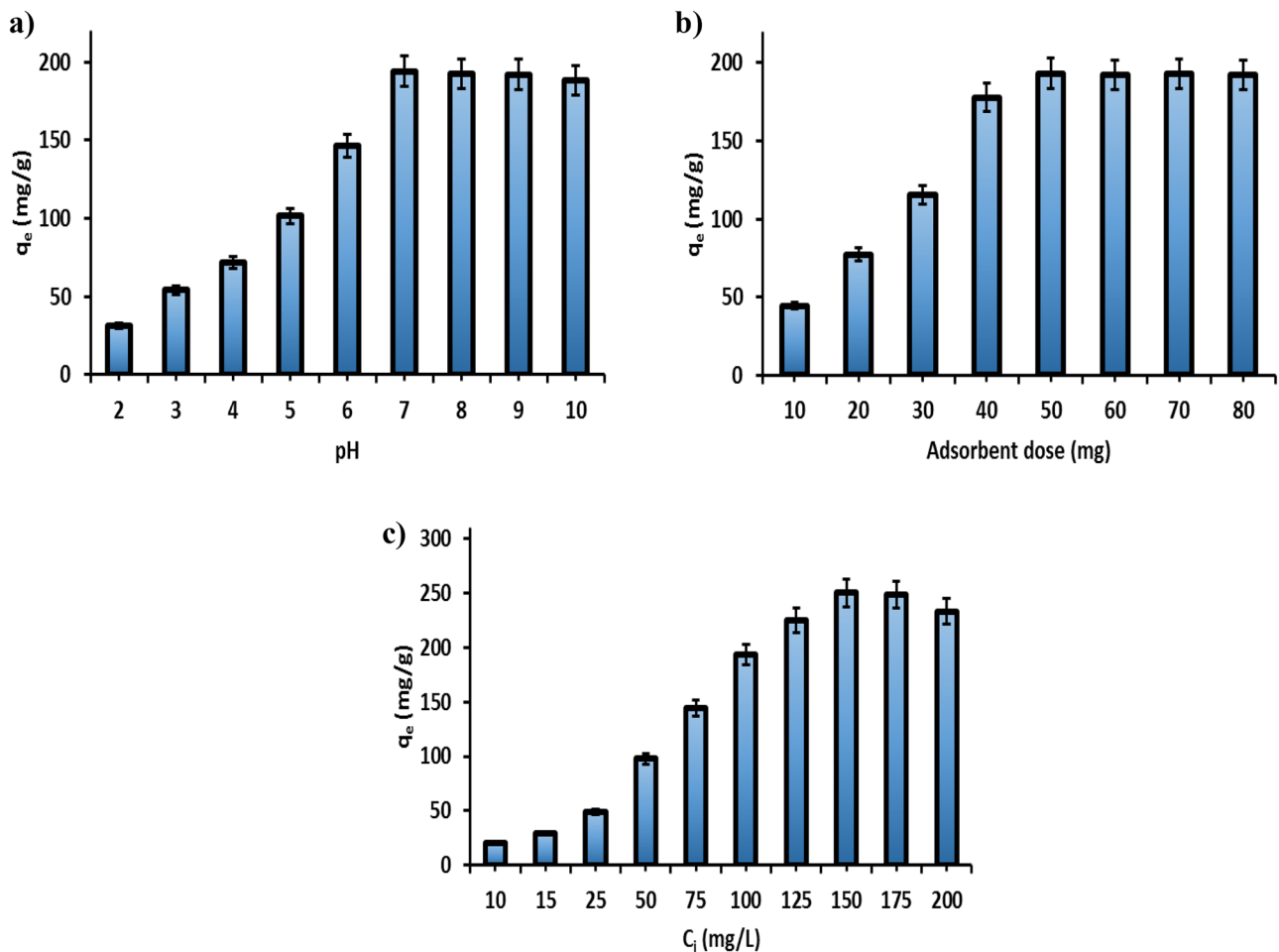


Fig. 9 The quantities of MB dye adsorbed (q_e (mg/g)) by PpAP/starch/GO ternary nanocomposites from aqueous solution according to **a)** initial pH; **b)** adsorbent dose; and **c)** initial MB dye concentra-

tion (C_i (mg/L)). The sorption time was 60 min and the temperature was 298 K in all experiments

studies have attributed this behaviour to the greater concentration gradient between MB molecules and adsorbents, which accelerates diffusion of dye onto the adsorbent surface and increases adsorption capacity [48]. Therefore, in adsorbate-adsorbent systems, initial pollutant concentration plays an important role in the quantity of pollutant adsorbed. This is demonstrated by our PpAP/Starch/GO ternary nanocomposites, where the quantities of MB dye adsorbed (q_e (mg/g)) increased from 19.9 to 233.2 as the initial MB dye concentration was increased from 10 mg/L to 200 mg/L (Fig. 9c).

Influence of sorption time

Sorption time is considered to be an influencing factor in the dye adsorption process [49]. Figure 10 shows the relationship between the adsorption capacity for MB dye on PpAP/Starch/GO ternary nanocomposites and sorption time at different initial MB dye concentrations (10, 75, and 150 mg/L).

It is demonstrated in Fig. 10 that the adsorption capacity of MB dye via PpAP/Starch/GO ternary nanocomposites improves with increasing sorption time, ultimately

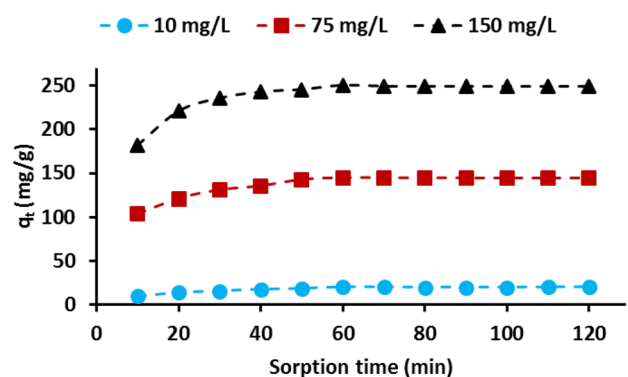


Fig. 10 The adsorption capacity of PpAP/Starch/GO ternary nanocomposites for MB dye adsorption from aqueous solution at different sorption times (conditions: initial pH 7; dose = 50 mg; V = 100 mL; initial C_{MB} = 10, 75, and 150 mg/L; T = 298 K)

reaching a maximum. The adsorption process was split into two time periods. The first ranged from 10 to 60 min over which time the equilibrium level was reached, and which is termed the rapid adsorption period. Over this period, the binding between the MB dye molecules and the functional groups and active sorption sites on the PpAP/Starch/GO ternary nanocomposite adsorbent reached its equilibrium. The adsorption rate of the MB dye was regulated by the rate at which the MB dye could transfer from the liquid onto the surface of the adsorbent particles of the ternary nanocomposites. The second period is termed the slow adsorption period. After 60 min sorption time, the sorption rate reduced progressively towards an asymptote. This was due to the binding between MB dye molecules and functional groups, as well as the active adsorption sites on the PpAP/Starch/GO ternary nano-adsorbents becoming essentially saturated. The rate of MB dye adsorption was dominated by the rate at which the MB dye was transferred from the external to the internal pore sites of the adsorbent particles of the nanocomposite [50]. Moreover, due to the relationship between sorption time and adsorption capacity for MB dye, the sorption time for the following tests was set to 60 min.

Kinetics modelling study

Various types of kinetic models such as pseudo-first-order, pseudo-secondary, Elovich models, and intraparticle diffusion models were employed to evaluate the kinetics of the adsorption of MB dye onto the PpAP/Starch/GO ternary nanocomposite, as reported in Table 2. The above kinetic models were applied at three different initial MB dye concentrations of 10, 75, and 150 mg/L, as per Fig. 11(a, b, c, d). The theoretical results obtained from the kinetic models are reported in Table 3, which shows that the pseudo-second-order kinetic model provided higher correlation coefficient values ($R^2 > 0.99$). Furthermore, the adsorption capacities calculated from the pseudo-second order model ($q_{cat} = 21.92, 149.2$ and 256.4 mg/g) show better agreement with the experimental adsorption capacities ($q_{exp} = 19.90, 144.6$ and 250.2 mg/g) compared to those obtained from the pseudo-first-order model. The pseudo-second-order rate constant (k_2) showed a decrease (0.00416 to 0.0014 mg/g min) when the initial MB dye concentration was increased (10 to 150 mg/L) due to reduced competition for surface adsorption sites at low MB dye concentrations. Therefore, at higher initial MB dye concentrations, there will be increased competition for adsorption sites on the surface of the ternary

Table 2 Different types of kinetics and isotherm models

Model	Linear Equation	Plot	References
Kinetics model equations			
^a Pseudo-first-order	$\ln(q_e - q_t) = \ln q_e - k_1 t$	$\ln(q_e - q_t)$ vs. t	[57]
^b pseudo-second-order	$\frac{t}{q_t} = \frac{1}{k_2 q_e^2} + \frac{t}{q_e}$	$\frac{t}{q_t}$ vs. t	[58]
^c Elovich	$q_t = \frac{1}{\beta} \ln(\alpha\beta) + \frac{1}{\beta} \ln t$	q_t vs. $\ln t$	[59]
^d Intraparticle diffusion	$q_t = K_{ip} t^{0.5} + F$	q_t vs. $t^{0.5}$	[60]
Isotherm model equations			
^e Langmuir	$\frac{C_e}{q_e} = \frac{C_e}{q_m} + \frac{1}{q_m K_L}$	$\frac{C_e}{q_e}$ vs. C_e	[61]
^f Freundlich	$\ln q_e = \ln K_F + \frac{1}{n} \ln C_e$	$\ln q_e$ vs. $\ln C_e$	[62]
^g Temkin	$q_e = A + B \ln C_e$	q_e vs. $\ln C_e$	[63]

^a q_e and q_t : the quantities of adsorbate adsorbed by the adsorbent (mg/g) at equilibrium and time t (min), respectively; k_1 : the pseudo first order rate constant (min^{-1})

^b k_2 : the pseudo-second-order rate constant (mg/g min); initial sorption rate (h) (mg/g min) calculated from $h = K_2 \times q_e^2$

^c α : the initial adsorption rate constant (mg/g. min); β : desorption rate constant (g/mg)

^d k_{ip} : intraparticle diffusion rate constant (mg/g $\text{min}^{0.5}$); F : a constant calculated from the intraparticle diffusion equation (mg/g)

^e q_e : the quantity of MB dye adsorbed using the adsorbent at equilibrium (mg/g); C_e : the concentration of adsorbate at equilibrium (mg/L); q_{max} : the maximum adsorption capacity, as calculated from the Langmuir isotherm model (mg/g); K_L : Langmuir constant (L/mg)

^f K_F : Freundlich constant (mg/g (L/mg)^{1/n}); n : heterogeneity constant

^g B : the heat of sorption constant (J/mol); A : Temkin constant (L/g)

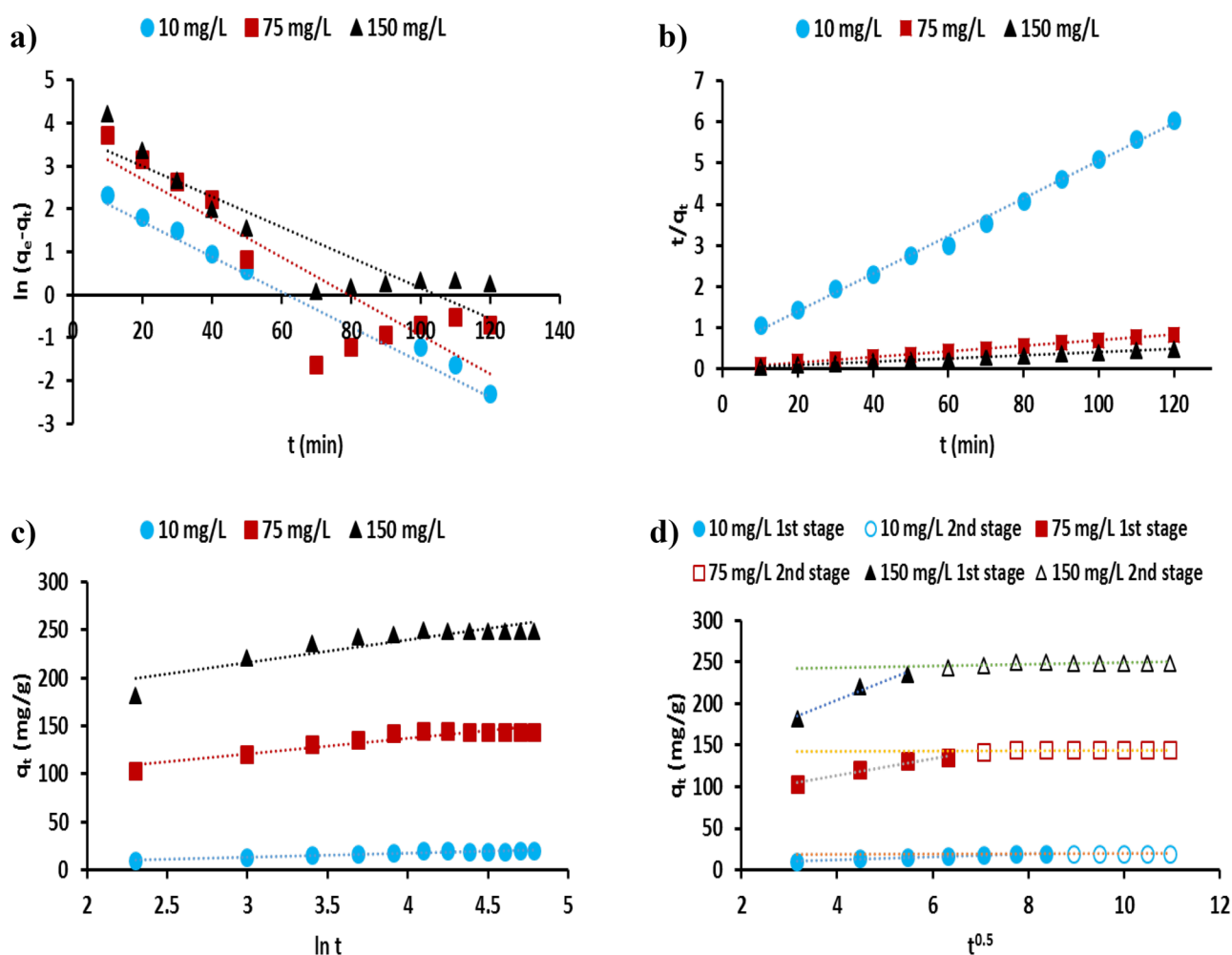


Fig. 11 Adsorption kinetics curve fitting for MB dye with PpAP/starch/GO ternary nanocomposite adsorbent: **a)** pseudo-first-order model; **b)** pseudo-second-order model; **c)** Elovich model; and **d)** intraparticle diffusion model

adsorbent nanocomposites and thus the associated rate constants will be low [51]. Also, the initial absorption rate (h) showed an increase of 2.0004 mg/g min to 95.238 mg/g min when the initial MB dye concentration was increased from 10 mg/L to 150 mg/L. This can be attributed to an increasing driving force to the mass transfer that allows more MB dye molecules to reach the surface of the ternary adsorbent nanocomposites in a given period of time [52]. A total adsorption system can be ‘organised’ into single or multiple phases comprising bulk diffusion, external diffusion, and intraparticle pore diffusion, as well as surface adsorption. The powerful stirring method effectively removes bulk diffusion, and in any case surface adsorption occurs quickly [53, 54].

In this investigation, the model describing intraparticle diffusion can be used to explain the diffusion mechanism during the adsorption reaction period. When q_t vs. $t^{0.5}$ provides a single line graph, the adsorption system is dominated by the diffusion mechanism; however, when several

linear sections are found in this graph, the adsorption system is determined by different mechanisms [55]. Plots of q_t vs. $t^{0.5}$ for the adsorption of MB dye on ternary PpAP/Starch/GO nanocomposites are presented in Fig. 11d. This figure shows that the MB dye adsorption system is regulated by the intraparticle diffusion mechanism due to the fact that these graphs not only contain a single straight line but also do not intersect the origin. Thus, for MB dye adsorption using three initial dye concentrations, two distinct straight lines appear in the intraparticle diffusion model graphs (q_t vs. $t^{0.5}$). The initial straight-line segment (an initial sharpest segment) shows that diffusion determined the mechanism and the MB dye diffused on the exterior surface of the ternary PpAP/Starch/GO nanocomposites with rate constants (k_{ip1}) of 1.967 g/mg/min^{0.5}, 10.198 g/mg/min^{0.5}, and 23.387 g/mg/min^{0.5} for the three initial MB dye concentrations (10, 75, and 150 mg/L, respectively). The second straight line segment

Table 3 Adsorption pseudo-first-order, pseudo-second-order, Elovich, and intraparticle diffusion kinetics parameters for MB dye adsorption by the PpAP/Starch/GO adsorbent (conditions: initial pH 7; dose=50 mg; initial C_{MB}= 10, 75, and 150 mg/L; V = 100 mL; T=298 K)

Kinetic models	Parameter	Initial MB dye concentration		
		10 mg/L	75 mg/L	150 mg/L
Pseudo-first-order	q _m (exp.) (mg/g)	19.90	144.6	250.2
	k ₁ (1/min)	0.041	0.045	0.035
	q _e cal.(mg/g)	12.61	36.40	41.24
	R ²	0.9134	0.7638	0.8224
Pseudo-second-order	k ₂ (mg/g.min)	0.0041	0.0017	0.0014
	q _e cal.(mg/g)	21.92	149.2	256.4
	h (mg/g min)	2.000	38.46	95.23
	R ²	0.9965	0.9993	0.9996
Elovich	α (mg/g.min)	5.6463	1525.6	11,556.6
	β (g/mg)	0.2425	0.0622	0.0424
	R ²	0.9160	0.8849	0.8027
Intraparticle diffusion	K _{ip} (mg/g.min ^{0.5})	1.1812	4.5368	6.4686
	F (mg/g)	8.5496	101.86	189.36
	R ²	0.8029	0.7541	0.6474

indicates an intraparticle diffusion mechanism with rate constants (k_{ip2}) of 0.117 g/mg/min^{0.5}, 0.206 g/mg/min^{0.5}, and 0.987 g/mg/min^{0.5} for these same three initial MB dye concentrations, (10, 75, and 150 mg/L), respectively [55].

The values of k_{ip1} were notably higher than those for k_{ip2}, suggesting that the rate of MB dye adsorption onto the ternary PpAP/Starch/GO nanocomposites was regulated by the exterior diffusion mechanism. The values of K_{ip} (defined as the intraparticle diffusion rate constant) and F (defined as the thickness of the boundary layer) computed from the slope and plot-intersection of q_t versus t^{0.5} are reported in Table 3. For the MB dye adsorption method, K_{ip} and F were found to increase with increasing initial MB dye concentration. The thickness of the boundary layer (F) increased due to the large amount of MB dye adsorbed onto it [56].

Isotherm modelling studies

Three common theoretical isotherm models, namely the Langmuir, Freundlich, and Temkin (Table 2), were used to investigate the nature of MB dye adsorption using PpAP/Starch/GO nanocomposites as ternary adsorbents (Fig. 12). The Langmuir theoretical isotherm model assumes that the exterior surface of the adsorbent is regular and homogeneous, with dye molecules forming a monolayer on the adsorption sites, and has been used to characterise physical and chemical adsorption mechanisms [50]. The Freundlich

theoretical model predicts a multilayer sorption process that can occur on irregular and heterogeneous surfaces of adsorbent, while the Temkin theoretical isothermal model can be used to explain the interaction forces between the adsorbate (i.e., MB molecules) and PpAP/Starch/GO ternary nanocomposites as adsorbents, as related to electrostatic attraction and ion exchange, and wherever the molecules in the layer will decrease more linearly with coverage than logarithmically [64].

The model factors computed for all theoretical isotherm models have been tabulated along with an associated R² to illustrate the model that provided the best fit in Table 4. According to the R² and maximum adsorption capacity (q_m) (as presented in Table 4), the theoretical Langmuir model showed a higher correlation with the data (R² > 0.99), and the adsorption capacities calculated via this model (q_m (cal.) = 243.9, 250.0, and 270.2 mg/g) were in good agreement with the experimental values of adsorption capacity (q_m (exp.) = 250.2, 258.6, and 278.6 mg/g) compared to the data obtained from the Freundlich and Temkin models. It was therefore concluded that the theoretical Langmuir model is the most appropriate to describe the MB adsorption process at different temperatures compared to the Freundlich or Temkin models. This indicates that the adsorption mechanism of cationic MB dye on PpAP/Starch/GO ternary nanocomposites is a monolayer adsorption system, in addition to the heat of adsorption being independent of surface coverage. By comparison, the isothermal Langmuir separation factor (R_L = 1/1 + K_LC_i) for MB dye was in the range of 0 < R_L < 1 (see in Table 4), which indicates that adsorption by PpAP/Starch/GO ternary nanocomposites is favourable.

Thermodynamic factors for the adsorption of MB dye onto ternary nanocomposites

Basic thermodynamic factors such as enthalpy change (ΔH°), entropy change (ΔS°), and Gibbs free energy change (ΔG°) have been determined for the MB dye adsorption process via PpAP/Starch/GO ternary nanocomposites. The values of ΔH° and ΔS° were computed from the Van't Hoff Eq. (5) [65, 66]:

$$\ln(K_L) = -\frac{\Delta H^\circ}{RT} + \frac{\Delta S^\circ}{R} \tag{5}$$

where K_L is the Langmuir equilibrium constant (L/mg), R is the universal gas constant (8.314 J/mol K), and T is the absolute temperature (K). Using Fig. 13, the values of ΔH° and ΔS° were calculated from the gradient and intercept of the linear equation of ln(K_L) vs. 1000/T. ΔG° was calculated at each of the three temperatures considered (298, 310, and 320 K) using Eq. 6.

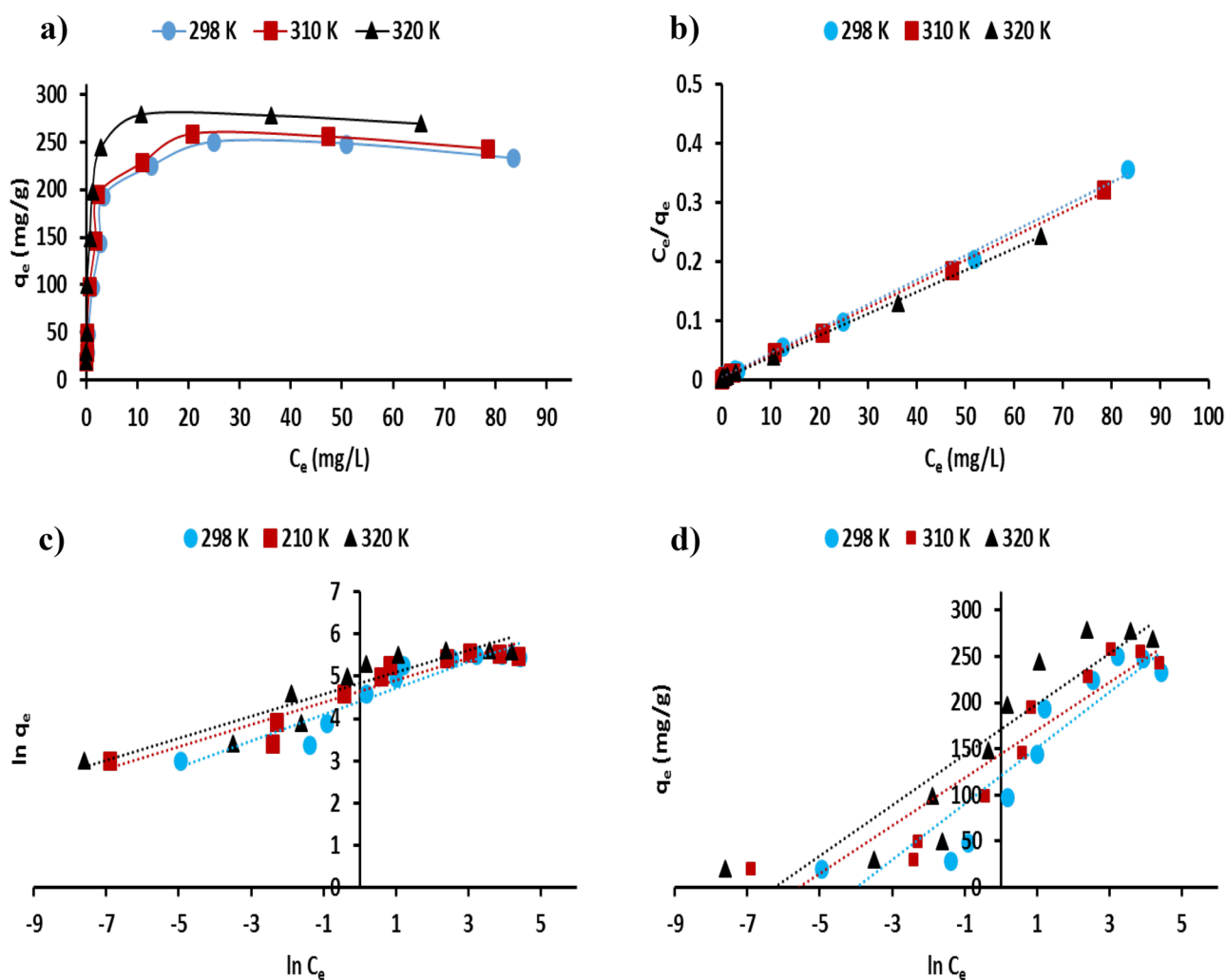


Fig. 12 a) Adsorption isotherms of MB dye onto the PpAP/starch/GO ternary nanocomposite adsorbent (conditions: initial pH 7; dose=50 mg; V=100 mL; sorption time=60 min; T=298, 310, and 320 K); fitting the adsorption isotherm plots of MB dye onto the

PpAP/starch/GO ternary nanocomposite adsorbent: b) Langmuir isotherm model; c) Freundlich isotherm model; and d) Temkin isotherm model

$$\Delta G^{\circ} = -RT \ln(K_L) \quad (6)$$

For the MB dye-PpAP/Starch/GO ternary nanocomposite system, ΔH° and ΔS° are estimated to be 44.49 kJ/mol and 150.02 J/mol K, respectively, while the ΔG° computed at each temperature was -0.1882 kJ/mol at 298 K, -2.058 kJ/mol at 310 K, and -3.481 kJ/mol at 320 K. These data indicate that the adsorption of MB dye onto PpAP/Starch/GO ternary nanocomposites confirms the endothermic as well as spontaneous nature of the system. Further, the MB dye adsorption process is more favourable at higher temperatures, whilst the positive value of the entropy change (ΔS°) indicates the decline in perturbation in the liquid–solid boundary system during the adsorption process.

MB dye adsorption mechanism

According to earlier work, the removal of organic impurities from polymer nanocomposites in liquid samples was a complex method that was determined via several chemical and physical attractive forces, including hydrogen bonding, electrostatic attraction, and π – π interactions [65, 67]. However, the main mechanisms are characterised by the distinctive features and behaviour of the adsorbents, as well as the adsorption environment. To study the removal of MB dye by the PpAP/starch/GO ternary nanocomposite, the mechanism of removal is predicted to be as follows (Fig. 4b). Firstly, hydrogen bonding will occur between the nitrogen atoms of the MB dye molecule and the oxygen

Table 4 Adsorption Langmuir, Freundlich, and Temkin model isotherm parameters for adsorption of MB dye onto the PpAP/starch/GO ternary nanocomposite adsorbent. (Conditions: initial pH 7; dose = 50 mg; V = 100 mL; sorption time = 60 min; T = 298, 310, and 320 K)

Isotherm models	Parameter	Temperatures of reaction		
		298 K	310 K	320 K
Langmuir	q_m (exp.) (mg/g)	250.2	258.6	278.6
	q_m (mg/g)	243.9	250.0	270.2
	K_L (L/mg)	1.078	2.222	3.700
	R_L range	0.004– 0.084	0.002– 0.043	0.001– 0.026
	R^2	0.9970	0.9987	0.9995
Freundlich	K_F (mg/g (L/mg) ^{1/n})	82.36	103.3	127.3
	n	3.188	3.796	3.832
	R^2	0.8868	0.9065	0.8681
Temkin	A	121.19	144.76	171.3
	B	30.313	25.917	27.412
	R^2	0.8560	0.8657	0.8374

atoms of oxygen-containing functional groups present on the surfaces of the ternary PpAP/starch/GO nanocomposite (Fig. 4b). Thus, this suggests a major role for hydrogen bonding in the MB dye removal mechanism. In addition, the adsorption system can be determined at a pH greater than the zero-point charge (pH_{pzc} 6) of the PpAP/Starch/GO ternary nanocomposites (Fig. 8); this is illustrated by the electrostatic interaction that can occur between the negative charge surface of the ternary nanocomposite adsorbent with the MB dye cations, indicating that the electrostatic interaction potentially contributed to the mechanism of removal of MB dye on PpAP/Starch/GO ternary nanocomposites. In addition, MB dye is a perfect planar molecule with an aromatic backbone and can thus be readily adsorbed onto the ternary PpAP/Starch/GO nanocomposites via π–π electron-donor interactions between the hexagonal structure of the PpAP/Starch/GO ternary nanocomposites and the planar aromatic structure of the MB dye. Confirmation of the above was gained through the data obtained from the FTIR study (Fig. 6).

Comparison of the adsorption capacity of several modern adsorbents

From the comparative results in Table 5 it can be shown that the maximum adsorption capacity (q_{max}) of the PpAP/Starch/GO ternary nanocomposite adsorbent is more efficient than the adsorbent materials listed in Table 5.

Influence of interfering media on the proportion of MB dye removal

Dye waste released into the environment usually contains various types of interfering media. Interfering media can lead to interference effects that frequently impact the adsorption mechanism. Figure 14 shows the effects of adding different types of interfering media such as organic dye materials (methyl orange, methyl red), ionic salts (Na₂SO₄, NaCl, KNO₃), and metal ions (Ni(II), Co(II), Pb(II)) at different concentrations ranging from 5 to 50 mg/L on the quantities

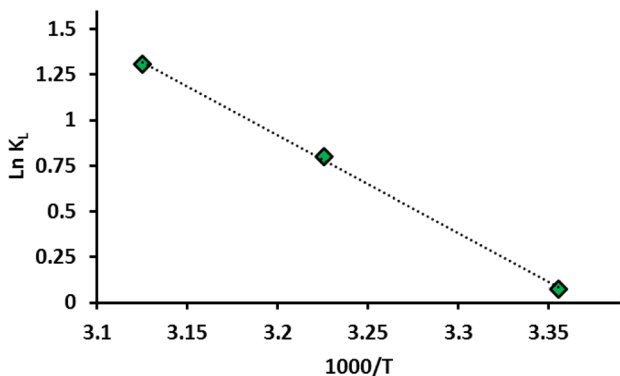


Fig. 13 Liner plot of ln K_L vs. 1000/T for MB dye adsorption onto the PpAP/Starch/GO ternary nanocomposite adsorbent

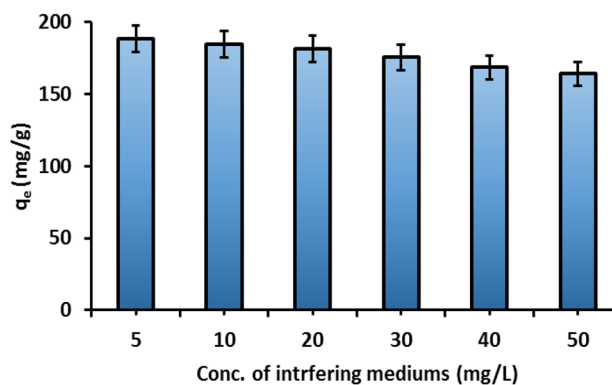


Fig. 14 Influence of interfering media concentrations on the quantities of adsorbed MB dye (q_e (mg/g)) for the PpAP/Starch/GO ternary nanocomposites adsorbent (conditions: initial pH 7; dose = 50 mg; initial C_{MB} = 100 mg/L; V = 100 mL; sorption time = 60 min; T = 298 K)

Table 5 Comparison of the adsorption capacity of several modern adsorbents with the ternary PpAP/Starch/GO nanocomposite with respect to MB dye removal

Adsorbents	Adsorption Capacity q_{\max} (mg/g)	References
Agar/k-carrageenan composite hydrogel	242.3	[46]
Wet-torrefied <i>Chlorella</i> sp. Microalgal biochar	113.0	[50]
Natural core-shell structure activated carbon beads (ACBs) from <i>Litsea glutinosa</i> seeds	29.03	[68]
Activated carbon (AC) modified by anionic surfactants—sodium lauryl sulfate (SLS)	232.5	[69]
Carboxymethyl Cellulose/Graphene Oxide Composite Aerogel (CMC/GO composite aerogel)	246.42	[70]
Polystyrene-acrylic/ZnO	150	[71]
Cow dung biochar (CDB)	17.5	
and domestic sludge biochar (SB)	19.2	
Coconut (<i>Cocos nucifera</i>) shell was chemically treated with sulfuric acid (H_2SO_4) to produce acid-fractionalised biosorbent	50.6	[72]
Chitosan-montmorillonite/polyaniline nanocomposite	111	[73]
Fe-modified banana peel	28.1	[74]
Electrospun oxime-grafted-polyacrylonitrile nanofiber	102.15	[75]
Polydopamine functionalised cellulose-MXene composite aerogel	168.93	[76]
Crosslinked poly(methacrylic acid)/organoclay nanocomposites	160	[77]
Bio-engineered copper nanoparticles	4.97	[78]
PpAP/Starch/GO ternary nanocomposites	250.2	This work

of adsorbed MB dye (q_e (mg/g)) by the PpAP/Starch/GO ternary nanocomposites, which was reduced from 188.4 to 164.2 by increasing the concentration of the interfering media from 5 mg/L to 50 mg/L. Previous work supports the supposition that metal ions co-exist with methylene blue or other dyes [79–82]. This decrease can be attributed to the neutralising effect of the surface charge of the ternary PpAP/Starch/GO adsorbent nanocomposites by the electrolyte species that contribute to the adsorption of MB dye-positive molecules on the outer surface of the adsorbent. However, this reduction in the proportion of MB dye removed is not fundamentally drastic, which shows that the PpAP/Starch/GO adsorbent can effectively remove MB dye from aquatic

samples, even in the presence of high concentrations of interfering media types. The above data from this study demonstrate that the PpAP/Starch/GO ternary nanocomposite adsorbent can perform efficiently in the field of dyestuff wastewater purification.

Recyclability assessment

The recyclability assessment was performed to evaluate the efficiency and stability of ternary PpAP/Starch/GO nanocomposites for adsorption of MB dye from different samples. The MB-loaded PpAP/Starch/GO ternary nanocomposites adsorbents were desorbed with 25 mL of anhydrous ethanol applied as the desorb solvent, in which the sorbent was shaken and then washed five times with distilled water (5×25 ml). Finally, the adsorbent was dried in a vacuum oven at 60 °C and reused for successive cycles. The adsorption and desorption cycle were completed six times periodically, where it was demonstrated that the quantities of MB dye adsorbed (q_e (mg/g)) by the PpAP/Starch/GO ternary nanocomposites reduced from 193.4 to 140.4 mg/g (Fig. 15).

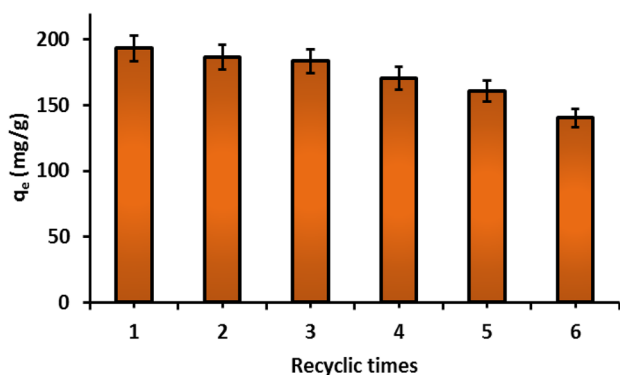


Fig. 15 Number of cycles of the PpAP/starch/GO ternary nanocomposite adsorbent when used for MB dye adsorption (conditions: initial pH 7; dose=50 mg; initial C_{MB} = 100 mg/L; V = 100 mL; sorption time = 60 min; T = 298 K)

Conclusion

In this study, several polymer composites of PpAP with/without Starch/GO were successfully synthesised by oxidative in situ polymerisation of the appropriate monomers in the presence of basic aqueous solutions using

ammonium persulfate as the initiator. PpAP@Starch (3:1) containing 8 wt% of GO was selected as the best adsorbent polymer composite to study the adsorption mechanism of methylene blue dye from aqueous solution using a batch adsorption mode. The interaction of starch and GO with the polymer was confirmed via FTIR, UV–Vis, and XRD characterisation. For the MB dye removal process, the proportion of MB dye removed by the PpAP/Starch/GO ternary nanocomposites was found to increase with increasing initial pH of the MB dye solution, adsorbent dose, initial MB dye concentration, sorption time, and temperature. A kinetics study implied a pseudo-second-order kinetic model ($R^2 > 0.996$) with different initial MB dye concentrations. It was demonstrated that the removal system is not only dominated by an intraparticle diffusion mechanism, but also by external diffusion. PpAP/Starch/GO ternary nanocomposites displayed a maximum adsorption capacity (q_m) of 250.2 mg/g for MB dye adsorption at a temperature of 298 K. The nanocomposites followed a Langmuir isotherm model ($R^2 > 0.997$) at different temperatures, which indicated the monolayer coverage of ternary nanocomposites with MB dye molecules. Thermodynamic measurements showed that the adsorption behaviour was spontaneous as well as an endothermic process. For the renewal of MB dye-loaded PpAP/Starch/GO ternary nanocomposites, the most appropriate solvent was anhydrous ethanol. From the results achieved in this study, the circulating PpAP/Starch/GO ternary nanocomposites can act as efficient and practical adsorbent substances for the removal of MB cationic dye from aqueous samples.

Supplementary information The online version contains supplementary material available at <https://doi.org/10.1007/s10965-022-03013-6>.

Acknowledgements The authors would like to thank the Universities of Koya and Kerbala for providing the required materials and instruments for this work. The authors would like to acknowledge Dr. Mark Watkins (University of Leicester) for helping and proofreading the manuscript.

Declarations

Competing Interest The authors declare that they have no known competing financial interests or personal relationships that could have appeared to influence the work reported in this paper.

References

- Kumar R, Sharma RK, Singh AP (2019) Synthesis and characterization of cellulose based graft copolymers with binary vinyl monomers for efficient removal of cationic dyes and Pb (II) ions. *J Polym Res* 26:135. <https://doi.org/10.1007/s10965-019-1790-9>
- Mohammed MQ, Ismail HK, Alesary HF, Barton S (2022) Use of a Schiff base-modified conducting polymer electrode for electrochemical assay of Cd (II) and Pb (II) ions by square wave voltammetry. *Chem Pap* 76:715–729. <https://doi.org/10.1007/s11696-021-01882-7>
- Mustafa FS, Güran M, Gazi M (2020) Effective removal of dyes from aqueous solutions using a novel antibacterial polymeric adsorbent. *J Polym Res* 27:247. <https://doi.org/10.1007/s10965-020-02227-w>
- Yasin SA, Zeebaree SYS, Sharaf Zeebaree AY, Haji Zebari OI, Saeed IA (2021) The efficient removal of methylene blue dye using CuO/PET nanocomposite in aqueous solutions. *Catalysts* 11:241. <https://doi.org/10.3390/catal11020241>
- Gupta VK (2009) Application of low-cost adsorbents for dye removal—a review. *J Environ manage* 90:2313–2342. <https://doi.org/10.1016/j.jenvman.2008.11.017>
- Jain H, Garg MC (2021) Fabrication of polymeric nanocomposite forward osmosis membranes for water desalination—A review. *Environ Technol Innov* 23:101561. <https://doi.org/10.1016/j.eti.2021.101561>
- Senguttuvan S, Senthilkumar P, Janaki V, Kamala-Kannan S (2021) Significance of conducting polyaniline based composites for the removal of dyes and heavy metals from aqueous solution and wastewaters-A review. *Chemosphere* 267:129201. <https://doi.org/10.1016/j.chemosphere.2020.129201>
- Thorat MN, Jagtap A, Dastager SG (2021) Fabrication of bacterial nanocellulose/polyethyleneimine (PEI-BC) based cationic adsorbent for efficient removal of anionic dyes. *J Polym Res* 28:354. <https://doi.org/10.1007/s10965-021-02702-y>
- Ardani MR, Pang AL, Pal U, Zheng R, Arsad A, Hamzah AA, Ahmadipour M (2022) Ultrasonic-assisted polyaniline-multiwall carbon nanotube photocatalyst for efficient photodegradation of organic pollutants. *J Water Process Eng* 46:102557. <https://doi.org/10.1016/j.jwpe.2021.102557>
- Koohi P, Rahbar-kelishami A, Shayesteh H (2021) Efficient removal of congo red dye using Fe₃O₄/NiO nanocomposite: Synthesis and characterization. *Environ Technol Innov* 23:101559. <https://doi.org/10.1016/j.eti.2021.101559>
- Reghioua A, Barkat D, Jawad AH, Abdulhameed AS, Khan MR (2021) Synthesis of Schiff's base magnetic crosslinked chitosan-glyoxal/ZnO/Fe₃O₄ nanoparticles for enhanced adsorption of organic dye: Modeling and mechanism study. *Sustain Chem Pharm* 20:100379. <https://doi.org/10.1016/j.scp.2021.100379>
- Gil A, Assis F, Albeniz S, Korili S (2011) Removal of dyes from wastewaters by adsorption on pillared clays. *Chem Eng J* 168:1032–1040. <https://doi.org/10.1016/j.cej.2011.01.078>
- Tony M (2020) Zeolite-based adsorbent from alum sludge residue for textile wastewater treatment. *Int J Environ Science Technol* 17:2485–2498. <https://doi.org/10.1007/s13762-020-02646-8>
- Elwakeel KZ (2009) Removal of Reactive Black 5 from aqueous solutions using magnetic chitosan resins. *J Hazard Mater* 167:383–392. <https://doi.org/10.1016/j.jhazmat.2009.01.051>
- Minitha C, Lalitha M, Jeyachandran Y, Senthilkumar L, Rajendra KRT (2017) Adsorption behaviour of reduced graphene oxide towards cationic and anionic dyes: Co-action of electrostatic and π - π interactions. *Mater Chem Phys* 194:243–252. <https://doi.org/10.1016/j.matchemphys.2017.03.048>
- Shang L, Bian T, Zhang B, Zhang D, Wu LZ, Tung CH, Yin Y, Zhang T (2014) Graphene-supported ultrafine metal nanoparticles encapsulated by mesoporous silica: robust catalysts for oxidation and reduction reactions. *Angew Chem* 126:254–258. <https://doi.org/10.1002/ange.201306863>
- Li Y, Du Q, Liu T, Sun J, Wang Y, Wu S, Wang Z, Xia Y, Xia L (2013) Methylene blue adsorption on graphene oxide/calcium alginate composites. *Carbohydr Polym* 95:501–507. <https://doi.org/10.1016/j.carbpol.2013.01.094>
- Vellaichamy B, Periakaruppan P, Nagulan B (2017) Reduction of Cr⁶⁺ from wastewater using a novel in situ-synthesized PANI/MnO₂/TiO₂ nanocomposite: renewable, selective, stable, and

- synergistic catalysis. *ACS Sustainable Chem Eng* 5:9313–9324. <https://doi.org/10.1021/acssuschemeng.7b02324>
19. Alesary HF, Ismail HK, Mohammed MQ, Mohammed HN, Abbas ZK, Barton S (2021) A comparative study of the effect of organic dopant ions on the electrochemical and chemical synthesis of the conducting polymers polyaniline, poly (o-toluidine) and poly (o-methoxyaniline). *Chem Pap* 75:5087–5101. <https://doi.org/10.1007/s11696-020-01477-8>
 20. Ismail HK, Alesary HF, Mohammed MQ (2019) Synthesis and characterisation of polyaniline and/or MoO₃/graphite composites from deep eutectic solvents via chemical polymerisation. *J Polym Res* 26:65. <https://doi.org/10.1007/s10965-019-1732-6>
 21. Sjahro N, Yunus R, Abdullah LC, Rashid SA, Asis AJ, Akhlisah Z (2021) Recent advances in the application of cellulose derivatives for removal of contaminants from aquatic environments. *Cellulose* 28:7521–7557. <https://doi.org/10.1007/s10570-021-03985-6>
 22. Mallakpour S, Ezhieh AN (2017) Preparation and characterization of chitosan-poly (vinyl alcohol) nanocomposite films embedded with functionalized multi-walled carbon nanotube. *Carbohydr Polym* 166:377–386. <https://doi.org/10.1016/j.carbpol.2017.02.086>
 23. Zare EN, Motahari A, Sillanpää M (2018) Nanoadsorbents based on conducting polymer nanocomposites with main focus on polyaniline and its derivatives for removal of heavy metal ions/dyes: a review. *Environ Res* 162:173–195. <https://doi.org/10.1016/j.envres.2017.12.025>
 24. Janaki V, Vijayaraghavan K, Oh BT, Lee KJ, Muthuchelian K, Ramasamy A, Kamala-Kannan S (2012) Starch/polyaniline nanocomposite for enhanced removal of reactive dyes from synthetic effluent. *Carbohydr Polym* 90:1437–1444. <https://doi.org/10.1016/j.carbpol.2012.07.012>
 25. Gomes RF, de Azevedo ACN, Pereira AG, Muniz EC, Fajardo AR, Rodrigues FH (2015) Fast dye removal from water by starch-based nanocomposites. *J Colloid Interface Sci* 454:200–209. <https://doi.org/10.1016/j.jcis.2015.05.026>
 26. Cheng R, Xiang B, Li Y, Zhang M (2011) Application of dithiocarbamate-modified starch for dyes removal from aqueous solutions. *J Hazard Mater* 188:254–260. <https://doi.org/10.1016/j.jhazmat.2011.01.104>
 27. Saberi A, Alipour E, Sadeghi M (2019) Superabsorbent magnetic Fe₃O₄-based starch-poly (acrylic acid) nanocomposite hydrogel for efficient removal of dyes and heavy metal ions from water. *J Polym Res* 26:27. <https://doi.org/10.1007/s10965-019-1917-z>
 28. Haroon M, Ullah R, Mehmood S, Haq F (2021) Synthesis and characterization of starch-g-poly methyl methacrylate and their properties as adsorbents for removing Rhodamine 6G from water. *J Polym Res* 28:330. <https://doi.org/10.1007/s10965-021-02692-x>
 29. Wang H, Duan M, Guo Y, Wang C, Shi Z, Liu J, Lv J (2018) Graphene oxide edge grafting of polyaniline nanocomposite: an efficient adsorbent for methylene blue and methyl orange. *Water Sci Technol* 77:2751–2760. <https://doi.org/10.2166/wst.2018.250>
 30. Gheydari M, Dorraji MS, Fazli M, Rasoulifard M, Almaie S, Daneshvar H, Ashjari HR (2021) Preparation of open-cell polyurethane nanocomposite foam with Ag₃PO₄ and GO: antibacterial and adsorption characteristics. *J Polym Res* 28:69. <https://doi.org/10.1007/s10965-021-02432-1>
 31. Zhang J, Azam MS, Shi C, Huang J, Yan B, Liu Q, Zeng H (2015) Poly (acrylic acid) functionalized magnetic graphene oxide nanocomposite for removal of methylene blue. *RSC Adv* 5:32272–32282. <https://doi.org/10.1039/C5RA01815C>
 32. Ali M, Husain Q, Sultana S, Ahmad M (2018) Immobilization of peroxidase on polypyrrole-cellulose-graphene oxide nanocomposite via non-covalent interactions for the degradation of Reactive Blue 4 dye. *Chemosphere* 202:198–207. <https://doi.org/10.1016/j.chemosphere.2018.03.073>
 33. Abd Ali L, Ismail HK, Alesary HF, Aboul-Enein H (2021) A nanocomposite based on polyaniline, nickel and manganese oxides for dye removal from aqueous solutions. *Int J Environ Sci Technol* 18:2031–2050. <https://doi.org/10.1007/s13762-020-02961-0>
 34. Hummers WS Jr, Offeman RE (1958) Preparation of graphitic oxide. *J Am Chem Soc* 80:1339–1339. <https://doi.org/10.1021/ja01539a017>
 35. Kar P, Pradhan NC, Adhikari B (2008) A novel route for the synthesis of processable conducting poly (m-aminophenol). *Mater Chem Phys* 111:59–64. <https://doi.org/10.1016/j.matchemphys.2008.03.012>
 36. Kojidi MH, Aliakbar A (2019) Synthesis of graphene oxide-based poly (p-aminophenol) composite and its application in solid phase extraction of trace amount of Ni (II) from aquatic samples. *Environ Monit Assess* 191:145. <https://doi.org/10.1007/s10661-019-7282-x>
 37. Verma SK, Choudhury A, Kar P (2015) Interaction of multi-walled carbon nanotube with poly (m-aminophenol) in their processable conducting nanocomposite. *Physica Status Solidi (a)* 212:2044–2052. <https://doi.org/10.1002/pssa.201431910>
 38. Usman A, Hussain Z, Riaz A, Khan AN (2016) Enhanced mechanical, thermal and antimicrobial properties of poly (vinyl alcohol)/graphene oxide/starch/silver nanocomposites films. *Carbohydr Polym* 153:592–599. <https://doi.org/10.1016/j.carbpol.2016.08.026>
 39. Thenmozhi G, Arockiasamy P, Santhi RJ (2014) Isomers of poly aminophenol: chemical synthesis, characterization, and its corrosion protection aspect on mild steel in 1 M HCl. *Int J Electrochem*. <https://doi.org/10.1155/2014/961617>
 40. Kong Y, Zhou Y, Shan X, Jiang Y, Yao C (2011) Electropolymerization of m-aminophenol on expanded graphite and its electrochemical properties. *Synth Met* 161:2301–2305. <https://doi.org/10.1016/j.synthmet.2011.08.038>
 41. Li R, Liu C, Ma J (2011) Studies on the properties of graphene oxide-reinforced starch biocomposites. *Carbohydr Polym* 84:631–637. <https://doi.org/10.1016/j.carbpol.2010.12.041>
 42. Ovchinnikov OV, Evtukhova AV, Kondratenko TS, Smirnov MS, Khokhlov VY, Erina OV (2016) Manifestation of intermolecular interactions in FTIR spectra of methylene blue molecules. *Vib Spectrosc* 86:181–189. <https://doi.org/10.1016/j.vibspec.2016.06.016>
 43. Alver E, Metin AÜ, Brouers F (2020) Methylene blue adsorption on magnetic alginate/rice husk bio-composite. *Int J Biol Macromol* 154:104–113. <https://doi.org/10.1016/j.ijbiomac.2020.02.330>
 44. Sousa HR, Silva LS, Sousa PAA, Sousa RRM, Fonseca MG, Osajima JA, Silva-Filho EC (2019) Evaluation of methylene blue removal by plasma activated palygorskites. *J Mater Res Technol* 8:5432–5442. <https://doi.org/10.1016/j.jmrt.2019.09.011>
 45. Pourjavadi A, Nazari M, Kabiri B, Hosseini SH, Bennett C (2016) Preparation of porous graphene oxide/hydrogel nanocomposites and their ability for efficient adsorption of methylene blue. *RSC Adv* 6:10430–10437. <https://doi.org/10.1039/C5RA21629J>
 46. Duman O, Polat TG, Diker CÖ, Tunç S (2020) Agar/κ-carrageenan composite hydrogel adsorbent for the removal of methylene blue from water. *Int J Biol Macromol* 160:823–835. <https://doi.org/10.1016/j.ijbiomac.2020.05.191>
 47. Lee LY, Gan S, Tan MSY, Lim SS, Lee XJ, Lam YF (2016) Effective removal of acid blue 113 dye using overripe cucumis sativus peel as an eco-friendly biosorbent from agricultural residue. *J Clean Prod* 113:194–203. <https://doi.org/10.1016/j.jclepro.2015.11.016>
 48. Sharma K, Dalai AK, Vyas RK (2018) Removal of synthetic dyes from multicomponent industrial wastewaters. *Rev Chem Eng* 34:107–134. <https://doi.org/10.1515/revce-2016-0042>
 49. Cui L, Wang Y, Gao L, Hu L, Yan L, Wei Q, Du B (2015) EDTA functionalized magnetic graphene oxide for removal of Pb (II),

- Hg (II) and Cu (II) in water treatment: adsorption mechanism and separation property. *Chem Eng J* 281:1–10. <https://doi.org/10.1016/j.cej.2015.06.043>
50. Yu KL, Lee XJ, Ong HC, Chen WH, Chang JS, Lin CS, Show PL, Ling TC (2021) Adsorptive removal of cationic methylene blue and anionic congo red dyes using wet-torrefied microalgal biochar: Equilibrium, kinetic and mechanism modeling. *Environ Pollut* 272:115986. <https://doi.org/10.1016/j.envpol.2020.115986>
 51. Kumar PS, Ramalingam S, Senthamarai C, Niranjana M, Vijayalakshmi P, Sivanesan S (2010) Adsorption of dye from aqueous solution by cashew nut shell: studies on equilibrium isotherm, kinetics and thermodynamics of interactions. *Desalination* 261:52–60. <https://doi.org/10.1016/j.desal.2010.05.032>
 52. Hameed B, Krishni R, Sata S (2009) A novel agricultural waste adsorbent for the removal of cationic dye from aqueous solutions. *J Hazard Mater* 162:305–311. <https://doi.org/10.1016/j.jhazmat.2008.05.036>
 53. Srivastava VC, Mall ID, Mishra IM (2006) Characterization of mesoporous rice husk ash (RHA) and adsorption kinetics of metal ions from aqueous solution onto RHA. *J Hazard Mater* 134:257–267. <https://doi.org/10.1016/j.jhazmat.2005.11.052>
 54. Wang S, Zhai YY, Gao Q, Luo WJ, Xia H, Zhou CG (2014) Highly efficient removal of acid red 18 from aqueous solution by magnetically retrievable chitosan/carbon nanotube: batch study, isotherms, kinetics, and thermodynamics. *J Chem Eng Data* 59:39–51. <https://doi.org/10.1021/je400700c>
 55. Singh SK, Townsend TG, Mazyck D, Boyer TH (2012) Equilibrium and intra-particle diffusion of stabilized landfill leachate onto micro- and meso-porous activated carbon. *Water Res* 46:491–499. <https://doi.org/10.1016/j.watres.2011.11.007>
 56. Crini G, Peindy HN, Gimbert F, Robert C (2007) Removal of CI Basic Green 4 (Malachite Green) from aqueous solutions by adsorption using cyclodextrin-based adsorbent: kinetic and equilibrium studies. *Sep Purif Technol* 53:97–110. <https://doi.org/10.1016/j.seppur.2006.06.018>
 57. Lagergren SK (1898) About the theory of so-called adsorption of soluble substances. *Sven Vetenskapsakad Handlingar* 24:1–39
 58. McKay G, Ho Y, Ng J (1999) Biosorption of copper from waste waters: a review. *Sep Purif Methods* 28:87–125. <https://doi.org/10.1080/03602549909351645>
 59. Elovich SY, Zhabrova G (1939) Mechanism of the catalytic hydrogenation of ethylene on nickel. I. Kinetics of the process. *J Phys Chem* 13:1761.
 60. Weber WJ Jr, Morris JC (1963) Kinetics of adsorption on carbon from solution. *J Sanit Eng Div* 89:31–59. <https://doi.org/10.1061/JSEDAI.0000430>
 61. Langmuir I (1916) The constitution and fundamental properties of solids and liquids. Part I. Solids *J Am Chem Soc* 38:2221–2295. <https://doi.org/10.1021/ja02268a002>
 62. Freundlich H (1907) Über die adsorption in lösungen. *Z Phys Chem* 57(1):385–470. <https://doi.org/10.1515/zpch-1907-5723>
 63. Tempkin M, Pyzhev V (1940) Kinetics of ammonia synthesis on promoted iron catalyst. *Acta Phys Chim USSR* 12(1):327
 64. Ali I, Alharbi OM, Allothman ZA, Badjah AY, Alwarthan A (2018) Artificial neural network modelling of amido black dye sorption on iron composite nano material: kinetics and thermodynamics studies. *J Mol Liq* 250:1–8. <https://doi.org/10.1016/j.molliq.2017.11.163>
 65. Maruthapandi M, Kumar VB, Luong JH, Gedanken A (2018) Kinetics, isotherm, and thermodynamic studies of methylene blue adsorption on polyaniline and polypyrrole macro-nanoparticles synthesized by C-Dot-Initiated polymerization. *ACS Omega* 3(7):7196–7203. <https://doi.org/10.1021/acsomega.8b00478>
 66. Li B, Guo J, Lv K, Fan J (2019) Adsorption of methylene blue and Cd (II) onto maleylated modified hydrochar from water. *Environ Pollut* 254:113014. <https://doi.org/10.1016/j.envpol.2019.113014>
 67. Cheng J, Zhan C, Wu J, Cui Z, Si J, Wang Q, Peng X, Turng LS (2020) Highly efficient removal of methylene blue dye from an aqueous solution using cellulose acetate nanofibrous membranes modified by polydopamine. *ACS Omega* 5:5389–5400. <https://doi.org/10.1021/acsomega.9b04425>
 68. Dao MU, Le HS, Hoang HY, Tran VA, Doan VD, Le TTN, Sirotkin A (2021) Natural core-shell structure activated carbon beads derived from *Litsea glutinosa* seeds for removal of methylene blue: Facile preparation, characterization, and adsorption properties. *Environ Res* 198:110481. <https://doi.org/10.1016/j.envres.2020.110481>
 69. Kuang Y, Zhang X, Zhou S (2020) Adsorption of methylene blue in water onto activated carbon by surfactant modification. *Water* 12:587. <https://doi.org/10.3390/w12020587>
 70. Zhu W, Jiang X, Jiang K, Liu F, You F, Yao C (2021) Fabrication of reusable carboxymethyl cellulose/graphene oxide composite aerogel with large surface area for adsorption of methylene blue. *Nanomaterials* 11:1609. <https://doi.org/10.3390/nano11061609>
 71. Pasichnyk M, Václavíková M, Melnyk I (2021) Fabrication of polystyrene-acrylic/ZnO nanocomposite films for effective removal of methylene blue dye from water. *J Polym Res* 28:56. <https://doi.org/10.1007/s10965-021-02418-z>
 72. Jawad AH, Abdulhameed AS, Mastuli MS (2020) Acid-fractionalized biomass material for methylene blue dye removal: a comprehensive adsorption and mechanism study. *J Taibah Univ Sci* 14:305–313. <https://doi.org/10.1080/16583655.2020.1736767>
 73. Minisy IM, Salahuddin NA, Ayad MM (2021) Adsorption of methylene blue onto chitosan–montmorillonite/polyaniline nanocomposite. *Appl Clay Sci* 203:105993. <https://doi.org/10.1016/j.clay.2021.105993>
 74. Çatloğlu F, Akay S, Turunç E, Gözmen B, Anastopoulos I, Kayan B, Kalderis D (2021) Preparation and application of Fe-modified banana peel in the adsorption of methylene blue: process optimization using response surface methodology. *Environ Nanotechnol Monit Manag* 16:100517. <https://doi.org/10.1016/j.enmm.2021.100517>
 75. Haider S, Binagag FF, Haider A, Al-Masry WA (2014) Electrospun oxime-grafted-polyacrylonitrile nanofiber membrane and its application to the adsorption of dyes. *J Polym Res* 21:371. <https://doi.org/10.1007/s10965-014-0371-1>
 76. Zhang T, Zhang W, Xi H, Li Q, Shen M, Ying G, Zhang J (2021) Polydopamine functionalized cellulose-MXene composite aerogel with superior adsorption of methylene blue. *Cellulose* 28:4281–4293. <https://doi.org/10.1007/s10570-021-03737-6>
 77. Zidan T, Yehia A, Abdelhamid AE (2021) Crosslinked poly (methacrylic acid)/organoclay nanocomposites: synthesis, characterization and methylene blue adsorption from aquatic environments. *J Polym Res* 28(8):306. <https://doi.org/10.1007/s10965-021-02665-0>
 78. Zeebaree SYS, Zeebaree AYS, Zebari OIH, Zebari AYS (2021) Sustainable fabrication, optical properties and rapid performance of bio-engineered copper nanoparticles in removal of toxic methylene blue dye in an aqueous medium. *Current Research in Green and Sustainable Chemistry* 4:100103. <https://doi.org/10.1016/j.crgsc.2021.100103>
 79. Nekouei F, Kargarzadeh H, Nekouei S, Keshtpour F, Makhlof ASH (2017) Efficient method for determination of methylene blue dye in water samples based on a combined dispersive solid phase and cloud point extraction using Cu (OH)₂ nanoflakes: central composite design optimization. *Anal Bioanal Chem* 409:1079–1092. <https://doi.org/10.1007/s00216-016-0026-7>
 80. Hassan SS, Nafady A, Solangi AR, Kalhor MS, Abro MI, Sherazi STH (2015) Ultra-trace level electrochemical sensor for methylene blue dye based on nafion stabilized ibuprofen derived gold nanoparticles. *Sens Actuators B Chem* 208:320–326. <https://doi.org/10.1016/j.snb.2014.11.021>

81. Liu X, An S, Wang Y, Yang Q, Zhang L (2015) Rapid selective separation and recovery of a specific target dye from mixture consisted of different dyes by magnetic Ca-ferrites nanoparticles. *Chem Eng J* 262:517–526. <https://doi.org/10.1016/j.cej.2014.10.002>
82. Xiao Z, Zhou J, Fan L, Li Y, He Y, Wang Y et al (2021) Controllable Preparation of Cu-MOF-Coated Carboxyl Filter Paper for Simultaneous Removal of Organic Dye and Metal Ions. *Ind Eng Chem Res* 60(19):7311–7319. <https://doi.org/10.1021/acs.iecr.1c00140>

Publisher's Note Springer Nature remains neutral with regard to jurisdictional claims in published maps and institutional affiliations.